pubs.acs.org/Biomac

Article

Carbosilane Glycodendrimers for Anticancer Drug Delivery: Synthetic Route, Characterization, and Biological Effect of Glycodendrimer–Doxorubicin Complexes

Monika Müllerová, Dina Maciel, Nádia Nunes, Dominika Wrobel, Marcel Stofik, Lucie Červenková Šťastná, Alena Krupková, Petra Cuřínová, Kateřina Nováková, Matěj Božík, Marek Malý, Jan Malý, João Rodrigues,* and Tomáš Strašák*

Cite This: *Biomacromolecules* 2022, 23, 276–290

Read Online

ACCESS | Metrics & More | Article Recommendations | Supporting Information

ABSTRACT: The complexity of drug delivery mechanisms calls for the development of new transport system designs. Here, we report a robust synthetic procedure toward stable glycodendrimer (glyco-DDM) series bearing glucose, galactose, and oligo(ethylene glycol)-modified galactose peripheral units. In vitro cytotoxicity assays showed exceptional biocompatibility of the glyco-DDMs. To demonstrate applicability in drug delivery, the anticancer agent doxorubicin (DOX) was encapsulated in the glyco-DDM structure. The anticancer activity of the resulting glyco-DDM/DOX complexes was evaluated on the noncancerous (BJ) and cancerous (MCF-7 and A2780) cell lines, revealing their promising generation- and concentration-dependent effect. The glyco-DDM/DOX complexes show gradual and pH-dependent DOX release profiles. Fluorescence spectra elucidated the encapsulation process. Confocal fluorescence microscopy demonstrated preferential cancer cell internalization of the glyco-DDM/DOX complexes. The conclusions were supported by computer modeling. Overall, our results are consistent with the assumption that novel glyco-DDMs and their drug complexes are very promising in drug delivery and related applications.

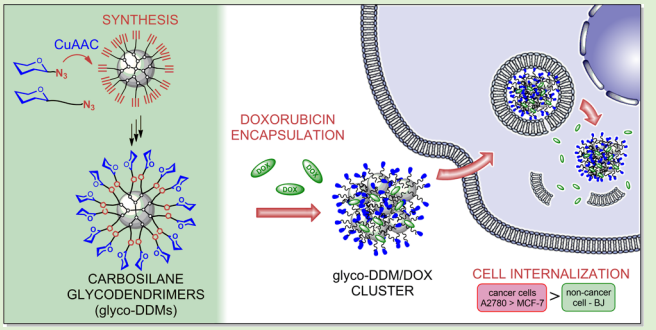

1. INTRODUCTION

Molecular recognition between carbohydrates and proteins promotes critical events in biological processes.[1−3] An interplay of multiple interactions of the individual sugar units attached to the nanoscale molecular scaffolds governs ionic and H-bond interactions to promote biological response and targeting. However, to a large extent, it is also responsible for the significantly reduced toxicity of the glycoconjugates compared to their molecular scaffolds. Synthetic glycoconjugates,[4] which emerged as useful tools in bionanotechnology[5−7] and biomedicine,[8−11] typically comprise systems with several copies of identical saccharide ligands attached to a biocompatible molecular,[4,12] polymeric,[4,8,13,14] or dendritic[15−18] scaffold. The synthetic control over the dendrimer (DDM) structure in terms of size, shape, and multivalency, together with the possibility to covalently introduce multiple ligands for targeting, increasing hydrosolubility, bioimaging, or physical encapsulation of drugs into their structural cavities, predetermines DDMs as optimal "glycocarriers" in nanomedicine. Moreover, the general stability, biocompatibility, and excellent water solubility of glycodendrimers (glyco-DDMs) increase their efficiency in drug delivery. Still, the complexity of mechanisms involved in biological processes challenges scientists to propose more efficient structural designs. Among others, glyco-DDMs based on polyamine,[19,20] polyester,[21] aromatic,[12] cyclotriphosphazene,[22] carbosilane,[23] or hybrid[24] scaffolds have been proposed to fit the needs of various bioapplications.

In cancer therapy, suppression of toxic side effects and the overall outcomes of the treatment depend on selective targeting of therapeutic compounds to cancer cells. As drug delivery systems (DDSs), dendritic compounds served as nanocarriers for various drugs with the capacity to improve their solubility and bioavailability and reduce the undesired toxic effect to nontarget tissues.[25] The dendritic structures provide a certain level of control over the properties of the encapsulated or complexed therapeutic moieties. The inclusion of hydrophobic therapeutics is typically achieved by mixing DDM and drug solution where the hydrophobic drug is

Received: September 24, 2021
Revised: December 5, 2021
Published: December 20, 2021

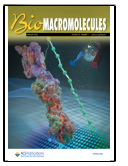

attracted to the nonpolar interior.[26] The release of the encapsulated molecules in an aqueous environment is passively controlled by a range of noncovalent interactions, including hydrophobic and electrostatic interactions, hydrogen bonding, and steric hindrance. To maximize the loading capacity of therapeutics within the DDM, the architecture of the host molecule must be carefully considered.

Recently, several studies have been conducted to design DDM-based nanocarriers that would improve drug stability and selectivity toward malignant tissues. Such high-molecular-weight nanoparticles can enhance anticancer efficacy while reducing the side effects, owing to properties including preferential accumulation in tumor tissue as a result of enhanced permeation and retention (EPR) effect[27] and active intracellular uptake.[28] The anthracycline doxorubicin (DOX), one of the most powerful chemotherapeutics, fights a wide range of cancers such as carcinomas, sarcomas, and hematological cancers.[29−31] Despite extensive application in clinical therapy, a remedy for numerous unfavorable aspects of the DOX treatment (severe cardiotoxicity; impact on the brain, kidney, liver, and other organs[32]) has not yet been found. Functionalized polyamidoamine (PAMAM),[33] polypropylenimine (PPI),[34] phosphoramidate,[35] and polylysine[36] based carriers loaded with DOX were designed to show tumor-selective activity[37] or to be used in combination therapy with other active species.[38,39] Surprisingly, only a little attention has been paid to therapeutic nanoconstructs comprising saccharide moieties. Specific carbohydrate units integrated into the DDM structure may serve not only as a biocompatible layer but also as a bioactive ligand for various bioreceptors of galectins and lectins in general, and glucose transporters overexpressed in abnormal cancer cell membranes. For example, galectin-1 and galectin-3 are engaged in angiogenesis-related processes and play a crucial role in the tumor cell interconnection.[40] Similarly, Seeberger and co-workers used a C-type lectin asialoglycoprotein receptor for hepatocyte-specific targeting. Galactosylated glycodendrimers with β-cyclodextrin cores efficiently delivered DOX into hepatocytes and induced apoptosis.[41] Agarwal et al.[34] synthesized dextran-conjugated PPI dendrimers as drug delivery units for site-specific delivery of DOX. The formulation was preferentially located in porous tumor vessels, where it efficiently released the DOX while not altering its chemical integrity. Despite the fundamental role of saccharide ligands in living organisms, to the best of our knowledge, only few nanocarriers of DOX based on saccharide ligands anchored to the dendritic scaffold have been investigated.

In this study, we developed a robust and flexible synthetic route to conjugate functional moieties of interest to the periphery of carbosilane dendrimers (CS-DDMs). To boost multivalent presentation, we tailored CS scaffolds with a derivative of 4-hydroxy isophthalic acid to double the amount of peripheral reactive sites. As we showed earlier,[42] introducing carbohydrate functional groups on the periphery of CS-DDM decreases its toxicity, while the hydrophobic CS core facilitates drug encapsulations. Therefore, we synthesized three series of 1st−3rd generation CS glyco-DDMs bearing gluco- and galacto-ligands conjugated to the molecule, directly or via a short oligo (ethylene glycol) (OEG) linker to further enhance the biocompatibility and hydrosolubility of the compounds.

DDMs in biological systems have consistently raised concerns because of inherent toxicity.[43] Compared to other dendritic drug delivery transporters, e.g., PAMAMs and PPIs, an advantageous aspect of our CS-based glyco-DDMs regarding toxicity is the absence of protonable or cationic groups within their structure. As positively charged groups significantly contribute to the compound's toxicity, uncharged CS glyco-DDMs may represent promising candidates for drug delivery without compromising the cell internalization process. Thus, we investigated the cytotoxicity of the glyco-DDMs toward both cancer (MCF-7 (breast) and A2780 (ovarian) and noncancer BJ cell line (human fibroblast cell type). Furthermore, glyco-DDM/DOX complexes were prepared to evaluate cytotoxicity, hematotoxicity, and DOX release studies. The cellular uptake and localization of the glyco-DDM/DOX complexes were inspected using confocal fluorescence microscopy, and the results were supported by computer modeling.

2. MATERIALS AND METHODS

2.1. Synthesis and Characterization of Glyco-DDMs. Literature procedures were followed in the preparation of allyl-terminated carbosilane DDMs.[44] The 3-iodopropyl-terminated G_1−G_3 CS-DDMs were prepared according to our previously reported method.[30,45] The 4-(methoxymethoxy)benzoic acid (**2**)[46] and acetylated galactose with the OEG linker (**18**)[47] were prepared adopting the reported procedure. Unless otherwise stated, 1-azido-1-deoxy-β-D-glucopyranoside tetraacetate (**16**), 1-azido-1-deoxy-β-D-galactopyranoside tetraacetate (**17**), bromomethyl methyl ether (MOMBr), sodium hydride (NaH), sodium hydroxide (NaOH), 2-propynyl amine, 1-hydroxybenzotriazole (HOBt), *N*,*N*′-dicyclohexylcarbodiimide (DCC), *N*-methylmorpholine (NMM), dimethylformamide (DMF), methyl 4-hydroxybenzoate, dimethyl 5-hydroxyisophtalate, potassium carbonate, $CuSO_4{\cdot}5H_2O$, sodium ascorbate, triethylamine, DOWEX 50 WX8, Amberlite IRA402, Chelex 100 (sodium form), and doxorubicin hydrochloride (DOX·HCl) were purchased from commercial sources and used without further purification.

NMR spectra were measured using a Bruker Avance 400 (^{1}H at 400.1 MHz; ^{13}C at 100.6 MHz; ^{29}Si {^{1}H} (INEPT technique) at 79.5 MHz) at 25 °C. ^{1}H and ^{13}C NMR signals of the prepared compounds were assigned to corresponding atoms utilizing gHSQC, gCOSY, and gHMBC 2D NMR correlation spectra. ^{1}H and ^{13}C chemical shifts (δ/ppm) are given relative to residual solvent signals (δ_H/δ_C: DMSO-*d6* 2.50/39.52); ^{29}Si spectra were referenced to external standard hexamethyldisilane (−19.87 ppm). HRMS spectra were measured using a MicroTOF-QIII instrument (Bruker Daltonics, Germany) with an ESI or APCI ionization source in positive mode. MALDI-TOF spectra of G_n-IPh-Glu, G_n-IPh-Gal, and G_n-IPh-OEG-Gal were measured using an UltrafleXtreme MALDI-TOF/TOF mass spectrometer (Bruker Daltonics, Germany) with a 1 kHz smartbeam II laser. The measurements of G_1-DDMs were done in positive reflectron mode, with the mass range 2−6 kDa. The measurements of G_2-DDMs were done in positive/negative linear mode, with the mass range 2−20 kDa. The accelerating voltage was set at 25 kV. Typically, spectra were obtained by accumulating 3000 shots. Dihydroxybenzoic acid was used as the matrix (10 mg/mL in acetonitrile/0,1% TFA 1:1). MALDI-TOF spectra of G_n-B-OEG-Gal and G_n-B-Glu series were measured using an Autoflex Speed (Bruker, DE) flexControl 3.4 (Build 135) on a spot of an MTP 384 ground steel BC target plate. Sample solution in THF (10^{-3} M) is used and mixed with matrixes, 2.5-DHB, HCCA, or dithranol. Elemental analysis was performed using an elemental analyzer FlashSmart CHNS/O from Thermo Scientific Inc.

Hereinbelow, representative abbreviations were used to refer to certain characteristics or structural motives of the compounds: G_n refers to the generation of the DDM, where n = 1, 2 or 3; B refers to **3** unit in the DDM structure; and IPh refers to **6** unit in the DDM structure.

2.1.1. Alkyne-Terminated Dendrimers: General Synthetic Procedure. Compounds **3** or **6** (1.1 equiv) and dry K_2CO_3 (1.3 equiv) were

https://doi.org/10.1021/acs.biomac.1c01264
Biomacromolecules 2022, 23, 276−290

suspended in dry DMF. The iodopropyl-terminated DDM (**7**, **8**, or **9**; 1 equiv; reactions were carried out in the 0.2−0.6 mmol scale) was dissolved in petroleum ether (35−60 °C fraction) and added dropwise to the suspension. The reaction mixture was stirred overnight at 80 °C. Then, after evaporating DMF under vacuum, the crude product was dissolved in methanol and filtered over a short silicagel column. The organic phase was evaporated (to ca. 3 mL volume) and purified using an organic solvent nanofiltration (OSN; see below) system. After evaporation to dryness, the product **10**, **11**, or **12** (91−93% yield) or **13**, **14**, or **15** (89−92% yield) was obtained as a brownish waxy solid.

2.1.2. Peripheral Attachment of Saccharide Moieties via CuAAC Click Reaction: General Synthetic Procedure. The alkyne-terminated DDM (**10**−**15**; 1 equiv; reactions were carried out in the 0.3−0.1 mmol scale) and the azide-functionalized saccharide moiety (**16**, **17**, or **18**; 1.2 equiv per branch) were dissolved in THF, and water was added (1:1). Then, an aqueous solution of $CuSO_4$ was added (1 equiv per branch) followed by the dropwise addition of a freshly prepared aqueous solution of sodium ascorbate (2 equiv per branch). The resulting solution was stirred overnight at room temperature. Then, after removing THF under vacuum, dichloromethane and an aqueous solution of ammonia were added. The mixture was stirred vigorously overnight to remove all the trapped Cu catalyst residues. The organic phase was washed twice with water, dried with magnesium sulfate, filtered, and evaporated under vacuum. The residue was purified using OSN (see below). After evaporation to dryness, the products **19a**−**33a** (84−93%) were obtained as brownish waxy solids.

2.1.3. OSN System. Organic solvent nanofiltration (OSN)[48] was carried out using solvent-resistant stirred cell Millipore (for 47 mm membranes) equipped with 1 kDa or 3 kDa MWCO regenerated cellulose ultrafiltration discs Millipore (Ultracel) and PTFE encapsulated O-rings Teflex (FEP/Viton, with nitrogen as a driving gas. Crude dendritic products were dissolved in 50 mL of an appropriate solvent (typically MeOH or MeOH/DCM mixtures up to 1:1 ratio) and passed through the membrane (5 mbar) until the residual volume of 5 mL of the retentate was reached. The retentate was then diluted with 45 mL of the same solvent mixture and filtered. ^{1}H NMR was used to monitor the purification progress. The procedure was repeated when necessary, but 3−4 cycles were typically sufficient to obtain analytically pure products.

2.1.4. Zemplén O-Deacetylation. To a solution of DDMs with 4, 8, and 16 peracetylated glycounits **19a**−**24a** (reactions were carried out in the 0.3−0.1 mmol scale) in MeOH, a catalytic amount of MeONa (1 M) was added, and the reaction mixture was stirred overnight. Then, to neutralize the solution, an ion exchange resin (Amberlite IRA402) was added. The solution was filtered and evaporated under vacuum to give **19b**−**24b** as glass-like solids or as brownish sticky waxy liquids (94−99% yield).

2.1.5. Accelerated Triethylamine-Catalyzed O-Deacetylation under Microwave Irradiation. DDMs with 8, 16, and 32 peracetylated glycounits **25a**−**33a** (reactions were carried out in the 0.3−0.1 mmol scale) were transferred to the microwave reaction vial (30 mL), suspended in distilled water (15−20 mL), and then, methanol (0.5 mL) and a catalytic amount of triethylamine (approx. 1 mg/10 mg of DDM) were added. The vial was sealed with a septum, placed into the microwave reactor cavity, and irradiated up to 55 °C with stirring (600 rpm) for 3 h. After cooling down to ambient temperature, the vial content was concentrated under reduced pressure. Completion of the deacetylation was checked using ^{1}H NMR and repeated in the same manner (for 1−2 h) when necessary. The products **25b**−**32b** yielded brownish puffy glass-like solids or brownish sticky waxy liquids (95−98% yield). The deacetylated glyco-DDMs were checked for the presence of Cu ions by ICP-OES. Products of insufficient purity were subsequently dissolved in water and treated with Chelex 100 (sodium form) until the complete removal of copper was achieved according to ICP-OES (detection limit 1−5 ppm Cu).

2.2. Cytotoxicity of Glyco-DDMs and Glyco-DDM/DOX Complexes. Cytotoxicity of the glyco-DDMs and glyco-DDM/DOX complexes was tested on both cancer (A2780 and MCF-7) and normal (BJ) human cell lines in a concentration range of 0.5−25 μM by the resazurin assay. MCF-7 cells (human Caucasian breast adenocarcinoma; acquired from the Leibniz Institute, DSMZ-German Collection of Microorganisms and Cell Cultures GmbH (Germany)) and A2780 (human ovarian carcinoma; acquired from the European Collection of Cell Cultures (ECACC)), (Manchester, UK) are commonly used to evaluate the therapeutic potential of the DOX comprising chemotherapy.[49,50] To evaluate selectivity toward cancer cells, we tested glyco-DDM/DOX complexes also on a normal cell line BJ, human foreskin fibroblast, kindly provided by Dr. William C. Hahn (Harvard Medical School). The cytotoxic effect of DDMs and glyco-DDM/DOX complexes was related to the DDM generation and concentration.

MCF-7 cells were regularly cultured and passaged in the cell culture dishes using the Roswell Park Memorial Institute (RPMI) 1640 Medium supplemented with 10% fetal bovine serum (FBS), 1% (v/v) antibiotic and antimycotic 100× solution (AA), 1% (v/v) nonessential amino acids 100× (NEAA), 1% (v/v) sodium pyruvate 100× (SP), and 10 μg/mL human insulin. A2780 cells were cultured and passaged in the cell culture dishes using the RPMI 1640 Medium supplemented with 10% FBS and 1% (v/v) L-glutamine (Glut) 100×. The BJ cell line was regularly cultured and passed on to the cell culture dishes using Dulbecco's Modified Eagle Medium (DMEM). All the reagents mentioned here were purchased from Fisher Scientific and Alfagene. The culture was maintained at 37 °C in a humidified incubator with 5% CO_2, and the medium was replaced every 2−3 days.

To investigate (i) cytotoxicity of the glyco-DDMs and (ii) therapeutic activity and selectivity of the glyco-DDM/DOX complexes to MCF-7, A2780, and BJ cell lines, 1 day before the experiments, cells were distributed into 96-well plates at a density of 1.5×10^4 cells per well in the complete medium (RPMI 1640 and/or DMEM). The next day, the medium was replaced with the fresh medium containing (i) 20 μL of the corresponding glyco-DDM or glyco-DDM/DOX complex in six different concentrations (0.5−25 μM) and (ii) free DOX·HCl or glyco-DDM/DOX complexes at the same DOX concentration (six concentrations; 0.5−25 μM). The glyco-DDMs, glyco-DDM/DOX complexes, and DOX·HCl were dissolved in water. After incubation at 37 °C for 48 h, the morphology of cells was checked using optical microscopy (Nikon Eclipse TE 2000E inverted microscope; 100× magnification). Then, the cell viability was quantified by measuring the metabolic activity of the cells in culture through the resazurin reduction assay. The cell culture medium was replaced with a fresh medium containing resazurin dye (7-hydroxy-3H-phenoxazin-3-one 10-oxide; 0.01 mg/mL), and the plates were kept at 37 °C in a cell incubator for 3 h. Subsequently, after aliquots of the cell supernatant were transferred to 96-well opaque plates, the resorufin fluorescence (λ_{ex} = 530 nm; λ_{em} = 590 nm) was measured using a microplate reader (Perkin-Elmer Victor^3 model 1420).

2.3. Encapsulation of DOX. Deacetylated glyco-DDMs **25b**−**33b** (10 mg) were dissolved in 3 mL of ultrapure water (UPW). Doxorubicin hydrochloride (DOX·HCl) in 10 molar excess to the dendrimers was dissolved in 300 μL of methanol. The DOX·HCl solution was neutralized by adding the corresponding amount of TEA (see Table S1). The dendrimer aqueous solution was then mixed with the DOX solution and stirred overnight vigorously (400 rpm) to allow the methanol to evaporate. Then, the aqueous mixture was centrifuged (5423 *g* for 10 min) to separate the noncomplexed excess of DOX. The supernatant was collected, and the precipitate was washed with UPW (5 mL) to wash out the whole amount of glyco-DDM/DOX complex (2 times). Then, the combined solutions were lyophilized to obtain the corresponding glyco-DDM/DOX complex. The precipitate (nonencapsulated free DOX) was redissolved in methanol (10 mL) and quantified via UV−vis spectroscopy to calculate the amount of encapsulated DOX by the dendrimer platform. The calculations were performed based on a standard calibration curve of the DOX.

2.4. Characterization of Hydrodynamic Size and Zeta Potential of Glyco-DDMs and Glyco-DDM/DOX Complexes.

https://doi.org/10.1021/acs.biomac.1c01264
Biomacromolecules 2022, 23, 276−290

Scheme 1. Synthesis of 4-Hydroxy-N-(prop-2-yn-1-yl)benzamide (3) and 5-Hydroxy-N,N-di(prop-2-yn-1-yl)isophtalamide (6) Branching Unit; (i) MOMBr and NaH, (ii) NaOH and MeOH, (iii) 2-Propynyl Amine, HOBt, DCC, NMM, and DMF, and (iv) DOWEX H^+ and MeOH

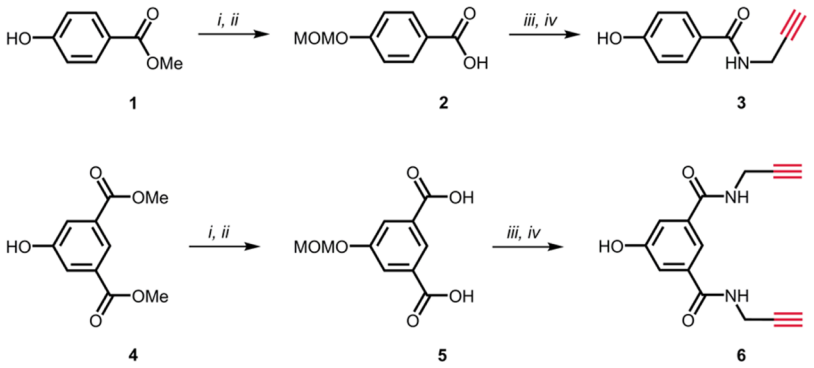

Particle sizes were measured using the dynamic light scattering (DLS) method in a Zetasizer Nano-ZS instrument (ZEN3600, Malvern Instruments, UK). The refraction factor was assumed to be 1.33, while the detection angle was 173° and the wavelength of the red laser light was 633 nm. The samples in distilled water and PBS (pH 7.4) were placed into the glass cell (PCS8501, Malvern) and measured at 25 °C. Data were analyzed using Malvern software. Particle charge measurements were conducted with a Zetasizer Nano-ZS using a combination of two measurement techniques: electrophoresis and laser Doppler velocimetry. The electrophoretic mobility of the particles was measured in an applied electric field using Malvern capillary plastic cells (DTS1070) with a copper electrode covered with gold. Samples were prepared and measured at 25 °C in water. The Zeta potential value was calculated using Malvern software (Version 7.13) from the Helmholtz−Smoluchowski equation. DDMs and their complexes with DOX were characterized using a 10 μM concentration for all measurements.

2.5. Fluorescence Spectra and Intensity of Glyco-DDM/DOX Complexes. Fluorescence spectra of the glyco-DDM/DOX complexes and DOX·HCl were measured in distilled water (10 μM concentration). Furthermore, excitation (310−540 nm) and emission (500−800 nm) spectra were recorded. An excitation slit was set to 4.0 nm for all measurements, whereas an emission slit was set to 4.5 nm.

2.6. Confocal Fluorescence Microscopy Studies of Cellular Internalization and Localization of Glyco-DDM/DOX Complexes. The interaction of glyco-DDM/DOX complexes with the cells, their cellular internalization, and localization were investigated by confocal fluorescence microscopy. Briefly, the cells were seeded in a sterile ibidi 18-well ibiTreat (tissue culture-treated surface) μ-Slide (part no. 81816) at the densities of 1.0×10^4 cells/well for the MCF7 cell line, 7.0×10^3 cells/well for the A2780 cell line, and 5.0×10^3 cells/well for the BJ cell line and cultured for 24 h. The cells were stained using a 4 μg/mL solution of Hoechst 33342 and incubated for 30 min in a 37 °C humidified atmosphere containing 5.0% CO_2. After washing the cells with DMEM, a solution of DOX or glyco-DDM/DOX complexes was added to obtain the final 10 μM concentration, and the cells were further incubated for 90 min in a 37 °C humidified atmosphere containing 5.0% CO_2. After the incubation period, the cells were washed with DMEM, and fluorescence images were acquired with a Leica CLSM SP8 microscope equipped with an HC PL APO CS2 20 × 0.75 DRY objective. A sequential scan mode was used to capture the blue and red channels with the following parameters: (i) the first sequence (blue channel) with 405 nm excitation and 410−480 nm emission for Hoechst 33342 (nucleus stain); (ii) the second sequence (red channel) with 488 nm excitation and 650−750 nm emission for DOX or glyco-DDM/DOX complexes. The images were processed using ImageJ software (version 1.52e).

2.7. Hematotoxicity of the Glyco-DDM/DOX Complexes. Three different blood samples obtained from Hospital Dr. Nélio Mendonça in Funchal, Madeira Island, were suspended in PBS (10% blood solution, pH 7.4). The blood solution (10 μL) was transferred into Eppendorf tubes, one for each compound/concentration to test, including a positive and negative control. Then, 70 μL of the glyco-DDM/DOX complex at two different concentrations (IC_{50} conc., 25 μM in PBS), 70 μL of UPW, and PBS for positive (C+) and negative (C−) controls, respectively, were added. To determine the total hemoglobin concentration in the blood samples, a 250-fold dilution of blood (PBS-untreated) in the C reagent (see the Supporting Information) was prepared (20 μL of blood in 5 mL of C reagent). All tubes were incubated at 37 °C for 3 h and then centrifuged at 3800 rpm for 10 min, and 40 μL of each supernatant was transferred to a 96-well plate containing the C reagent (160 μL) in each well. The absorbance was measured at 550 nm using the C reagent as blank (glyco-DDM/DOX complexes have no absorbance at 550 nm), and the values were used to calculate the amount of hemoglobin released in each tube and the respective percentage of hemolysis.

2.8. DOX Release Studies. The cumulative release (CR) profiles of DOX from the glyco-DDM/DOX complexes were determined using a dialysis method in the PBS medium of physiological pH (7.4) and acidic pH (5.0). Each sample (1 mg) was weighed into a dialysis vial (MWCO = 2000). To each vial, distilled water (200 μL) was added to dissolve the sample. Then, the vial was sealed and placed into a glass bottle with the PBS medium of pH 7.4 or 5.0 (10 mL) and incubated at 37 °C. In different time intervals, the solution (1 mL) was withdrawn, and the concentration of the released DOX was determined via UV−vis spectrophotometry (at 500 nm on an Evolution 220 UV−vis spectrophotometer, Thermo Scientific, USA) to calculate the CR percentage of DOX (see the Supporting Information). All experiments were conducted in triplicate.

2.9. Computer Modeling of Dendrimers and Their Complexes with Doxorubicin. 3D computer models of DDMs were created using a dendrimer builder implemented in the Materials Studio software package (BIOVIA, San Diego, CA). DOX structure was obtained from https://www.dsf.unica.it/translocation/db/doxorubicin.html. Generalized amber force field (GAFF)[51] was used for parameterization of DOX, while GAFF and GLYCAM 06j[52] force fields were used for parameterization of glyco-DDMs. The RESP technique[53] was used to calculate partial charges of DDMs and DOX atoms. The pmemd.cuda module[54] from the Amber18 package[55] was used for molecular dynamics simulations (explicit water, NPT, P = 1 bar, T = 298 K, length of simulation 150 ns (one DDM systems) and 200 ns (two DDM systems)). The MM/PBSA method[56] was used to estimate the free energies of binding $\Delta G = \Delta H - T\Delta S$. More information is provided in the Supporting Information and references therein.[53,57−67]

2.10. Data Evaluation and Statistics. Statistical analysis of cytotoxicity, hematotoxicity, encapsulation, and drug release data was performed using GraphPad software (La Jolla, CA). Results were expressed as mean ± standard error of the mean (SEM). IC50 values were estimated by the GraphPad program using nonlinear regression.

https://doi.org/10.1021/acs.biomac.1c01264
Biomacromolecules 2022, 23, 276−290

Scheme 2. Synthetic Route toward CS Dendritic Compounds for the Multivalent Presentation of Functionalities at the Periphery Comprising Alkyne-Terminated CS-DDMs and CS Glyco-DDMs; (v) 3 or 6, K_2CO_3, DMF, (vi) 16, 17, or 18, $CuSO_4 \cdot 5H_2O$, Sodium Ascorbate, THF, Water, (vii) Et_3N, MeOH, Water, and MW[a]

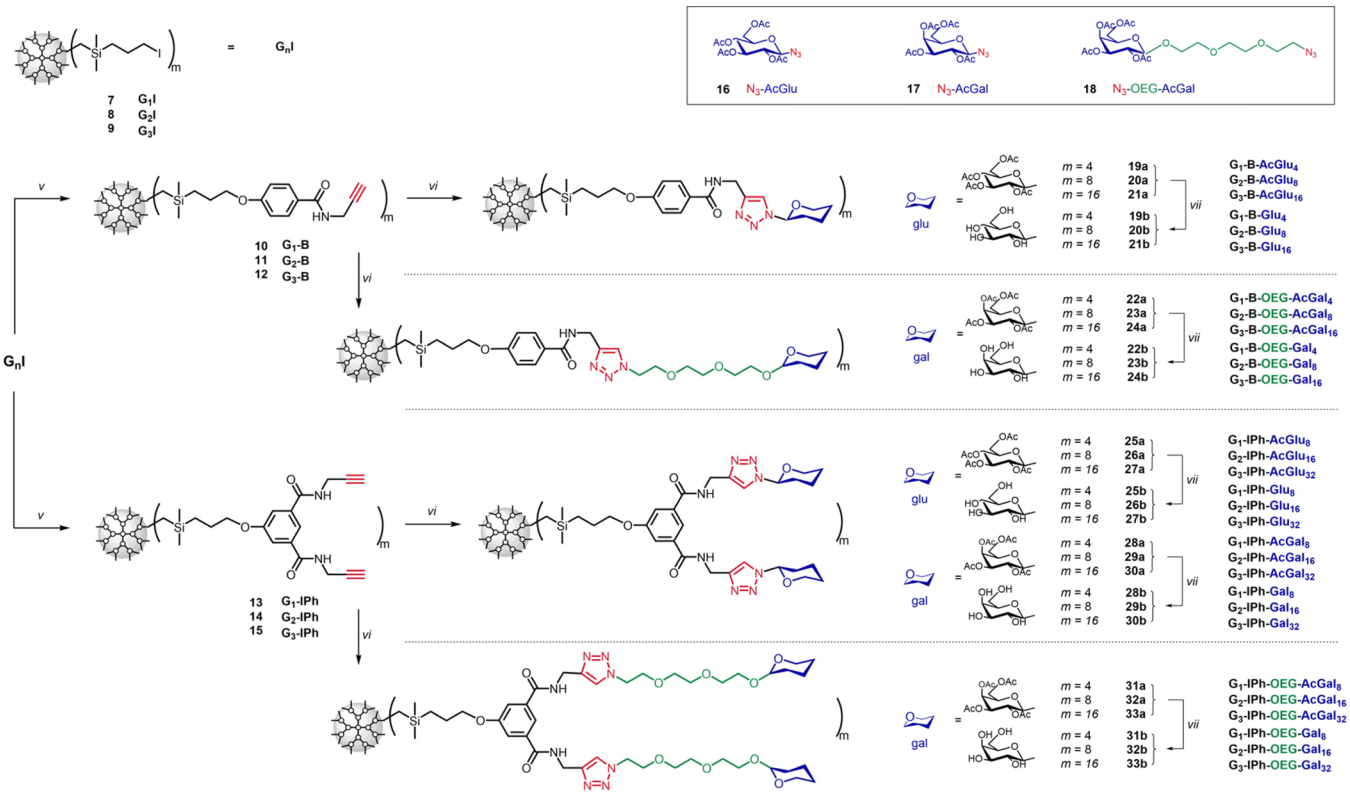

[a]For full glyco-DDM structures, see Scheme S1.

3. RESULTS AND DISCUSSION

3.1. Synthesis and Characterization of Glyco-DDMs.

Novel phenolic alkynes designed to introduce triple bonds on the periphery of CS-DDMs were prepared in two synthetic steps from commercially available substrates **1** and **4** (Scheme 1). To control the density of the peripheral units, alternatives of CS-DDMs with one (**3**) and two (**6**) alkynes per dendritic branch were synthesized.

Alkyne-terminated CS-DDMs **10**−**12** were synthesized by nucleophilic substitution of iodine by a phenolic group of **3** in the presence of a mild base. To boost multivalency, analogues **13**−**15** with substrate **6** (doubled amount of peripheral triple bonds) were prepared using the same method. Completion of the reaction was confirmed by observing a shift of the indicative triplet signal from 3.18 (methylene triplet next to iodine) to 3.85−3.98 ppm (methylene triplet next to the newly formed ether oxygen) in ^{1}H NMR spectra. We used copper(I)-catalyzed azide-alkyne cycloaddition (CuAAC) to attach the saccharide moieties to the periphery. As we verified recently,[42,68] this procedure represents a facile method for the peripheral functionalization of the CS-DDMs, providing pure products in excellent yields. The disappearance of an indicative signal of the propargyl group methine proton (3.05−3.12 ppm) and a formation of uniform singlet of triazole proton (7.93−8.24 ppm) indicated quantitative derivatization of terminal triple bonds with the azide group comprising saccharide derivatives. The efficient removal of copper ions was checked using ICP-OES. However, the reaction is typically carried out in excess of saccharide reagent (1.3 equiv). Based on our experience, chromatographic purification of DDMs may be challenging, especially in higher generations. At least, it is usually associated with a considerable mass loss. Thus, we took advantage of a substantial size difference between the reagent and the product to remove the unreacted saccharide derivative using nanofiltration. The separation of crude products dissolved in the MeOH/DCM mixture by nanofiltration proved to be an elegant, harmless, and high-yielding purification method that is, moreover, much faster and less solvent-demanding than generally used dialysis. Finally, the O-acetylated CS-glyco-DDMs **19a**−**24a** were deacetylated under Zemplén conditions (MeONa; MeOH). However, in the case of glyco-DDMs **25a**−**33a**, the deacetylation did not complete even after a prolonged reaction time. Therefore, an improved method of Meier et al.[69] based on triethylamine-catalyzed deacetylation under microwave irradiation was adopted to accelerate the deprotection process. The disappearance of the four separated singlets of acetyl groups around 2.0 ppm in ^{1}H NMR reliably indicated an efficient deacetylation. Finally, the NMR and MALDI-TOF MS analyses confirmed the proposed structures of both O-acetylated and deprotected G_1−G_3 glyco-DDMs (see the molecular structures in Scheme 2).

All glyco-DDMs are stable compounds; there was no structural degradation for a minimum of 28 days (in DMSO-d_6 solution) as confirmed via ^{1}H NMR analyses, (see Figure S2).

The glyco-DDMs with a higher degree of branching (**25b**−**33b**) were excellently soluble in water. Their UV−vis spectra (see Figure S1) show that these substances, unlike pure DOX, do not absorb in the 500 nm region. Thus, the UV−vis method

https://doi.org/10.1021/acs.biomac.1c01264
Biomacromolecules 2022, 23, 276−290

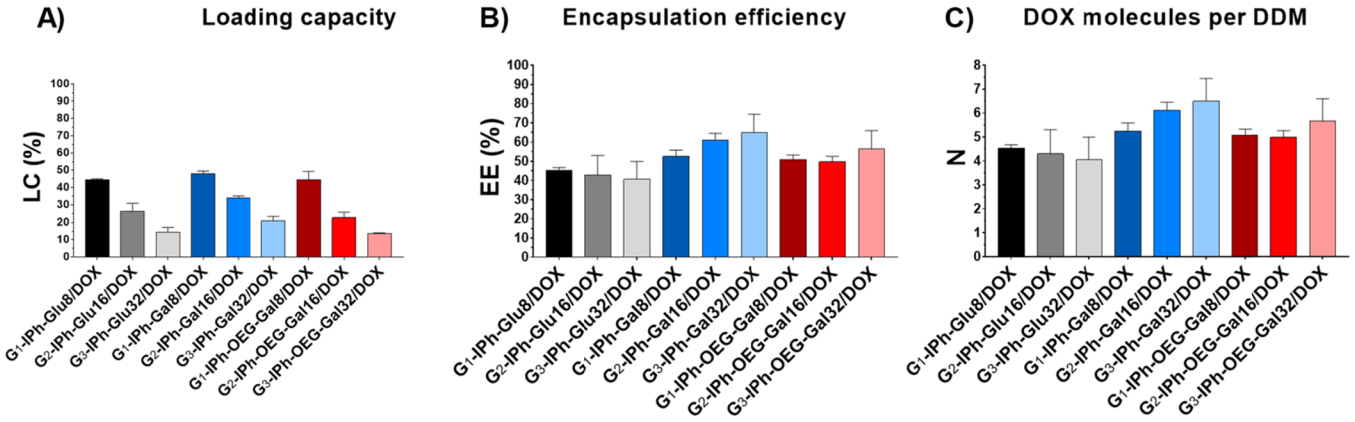

Figure 1. Encapsulation characteristics of glyco-DDM/DOX complexes (graphic representation): (A) loading capacity (LC), LC = $W_e/W_c \times 100$, where W_e is the weight of encapsulated DOX, and W_c is the weight of the DOX/DDM complex; (B) encapsulation efficiency (EE), EE = $W_e/W_t \times 100$, where W_e is the weight of encapsulated DOX, and W_t is a total DOX weight; (C) amount of DOX molecules per DDM (N), $N = n(\mathrm{DOX}_{\mathrm{encaps.}})/n(\mathrm{DDM})$, where $n(\mathrm{DOX}_{\mathrm{encaps}})$ is a molar quantity of encapsulated DOX and n(DDM) is a molar quantity of the DDM.

Table 1. Hydrodynamic Diameters (d_h) and Zeta Potential (ζ) of Glyco-DDMs and Glyco-DDM/DOX Complexes[a]

	d_h [nm] in water		d_h [nm] in PBS		ξ-values [mV]	
compound	DDM	DDM/DOX	DDM	DDM/DOX	DDM	DDM/DOX
G_1-IPh-Glu_8	8 ± 1	48 ± 11	7 ± 1	67 ± 6	2.9 ± 0.6	−17.7 ± 5.5
G_2-IPh-Glu_{16}	14 ± 2	45 ± 3	16 ± 2	82 ± 31	−16.0 ± 1.2	−4.2 ± 0.1
G_3-IPh-Glu_{32}	17 ± 3	350 ± 10	18 ± 6	320 ± 31	−1.2 ± 0.9	−9.5 ± 0.2
G_1-IPh-Gal_8	6 ± 1	9 ± 1	6 ± 1	11 ± 3	−0.3 ± 0.7	−7.4 ± 0.7
G_2-IPh-Gal_{16}	14 ± 3	14 ± 3	14 ± 1	11 ± 2	7.2 ± 0.9	−23.7 ± 4.2
G_3-IPh-Gal_{32}	17 ± 2	16 ± 2	8 ± 2	16 ± 1	−2.3 ± 1.5	1.1 ± 0.1
G_1-IPh-OEG-Gal_8	5 ± 2	86 ± 12	6 ± 2	86 ± 9	−5.3 ± 1.5	−9.3 ± 0.7
G_2-IPh-OEG-Gal_{16}	6 ± 1	71 ± 6	6 ± 1	70 ± 13	−4.5 ± 1.0	−1.6 ± 0.9
G_3-IPh-OEG-Gal_{32}	7 ± 1	5 ± 2	20 ± 2	6 ± 2	−7.5 ± 2.1	−1.4 ± 1.7

[a]Data are presented as mean ± SD.

of quantifying the amount of unencapsulated DOX is applicable. Unfortunately, the solubility of their less branched analogues **19b−24b** was insufficient for intended biochemical applications.

3.2. Cytotoxicity of Glyco-DDMs. In the range of tested concentrations, all glyco-DDM series across generations exhibit exceptionally high biocompatibility to both cancer and noncancer cell lines (see Figure S3). The viability of BJ cells is exceptionally high (>90%) in the tested concentration range (0.5−25 μM), indicating the absence of toxic effect on the noncancer cell line. Moreover, in MCF-7 and A2780 cancer cell lines, the cell viability did not drop under 80% compared to the control even when the highest concentration (25 μM) was dosed. The low cytotoxicity of our glyco-DDMs follows the general biocompatibility of glyco-DDMs demonstrated in numerous studies.[42,43,70,71] Despite being generally accepted that the DDM toxicity increases with the generation,[43,72,73] the biocompatibility of our glyco-DDMs is steadily stable in all generations. As we expected, our results indicate no significant difference in toxicity of the glyco-DDMs considering the stereoconfiguration of the saccharide moiety. In the G_n-IPh-OEG-Gal series, we would expect increased viability due to the presence of the OEG linker. Compared to G_n-IPh-Gal, the difference in toxicity of the G_n-IPh-OEG-Gal series is negligible. However, with biocompatibility above 85%, it is rather difficult to observe any significant improvement.

3.3. Encapsulation of DOX. When we used 10 molar excess of DOX, all DDM series across generations encapsulated resembling quantity of DOX (41−65%). In other words, all series and generations entrap a similar amount of DOX molecules per one DDM molecule (4−6), which is particularly interesting considering the size difference between generations. The loading capacity (LC) favors lower generations (LC of G_1 being roughly 2−3 times higher than that of G_3). Nevertheless, the loading capacities show minor differences across DDM series within the same generation, indicating a negligible influence of saccharide configuration or OEGylation levels on the encapsulation process (Figure 1; see Table S2 for numeric values).

These observations are probably related to the surface modification of the glyco-DDMs. With increasing generation, although the area inside the dendrimer molecule expands, the amount of surface groups is higher as well. With an increasing number of large peripheral glyco-units, a mechanical and/or chemical barrier for encapsulation may be created, limiting the number of encapsulated DOX molecules.

Nevertheless, the presence of large cluster/micellar structures rather than isolated glyco-DDMs in solutions has been found by DLS (Section 3.4). Therefore, with glyco-DDM clusters, the spatial availability of the higher generations to interact with the DOX molecules might be decreased compared to theoretical isolated glyco-DDM molecules. Consequently, the encapsulation efficiency of the three generations may be relatively similar despite the size disparity.

Hydrophobic interactions typically drive the inclusion of lipophilic drugs into nonpolar DDM interiors. However, both

https://doi.org/10.1021/acs.biomac.1c01264
Biomacromolecules 2022, 23, 276−290

Table 2. Calculated IC_{50} Values of the Glyco-DDM/DOX Complexes[a]

	IC_{50} (μM)									
		G_n-IPh-Glu/DOX			G_n-IPh-Gal/DOX			G_n-IPh-OEG-Gal/DOX		
	DOX	G_1	G_2	G_3	G_1	G_2	G_3	G_1	G_2	G_3
MCF-7	0.7 ± 0.1	24.9 ± 3.5	5.8 ± 0.8	2.8 ± 0.2	19.8 ± 3.1	13.2 ± 1.7	4.3 ± 0.7	>25.00[b]	5.3 ± 0.8	4.8 ± 0.6
A2780	0.1 ± 0.0	4.0 ± 0.3	0.7 ± 0.1	0.3 ± 0.0	4.1 ± 0.7	3.1 ± 0.5	0.6 ± 0.1	31.6 ± 2.0	1.7 ± 0.1	1.1 ± 0.1
BJ	0.4 ± 0.1	58.3 ± 7.9	20.5 ± 2.1	2.3 ± 0.3	9.7 ± 1.1	11.7 ± 1.1	2.2 ± 0.2	20.1 ± 1.8	1.2 ± 0.2	0.8 ± 0.1

[a]Data are presented as mean ± SD. [b]IC_{50} value too high to determine the value accurately based on the used concentration range. Nonlinear regression—inhibitor vs normalized response was used in the calculations.

hydrophobic (CS interior) and hydrophilic (peripheral saccharide moieties) interactions between DOX and the glyco-DDMs were described by the shifts in the emission fluorescence maxima (Section 3.5) and, also, by computer modeling (Section 3.10). Thus, parameters governing the encapsulation process might be much more complex.

3.4. Characterization of Hydrodynamic Size and Zeta Potential of Glyco-DDMs and Glyco-DDM/DOX Complexes. The hydrodynamic diameters (d_h) of glyco-DDMs and glyco-DDM/DOX complexes were measured in water and PBS buffer (Table 1). In most cases, the glyco-DDM size increased with increasing dendrimer generation (in the size range of 5−20 nm). Dendrimers in PBS solution were slightly larger than those in pure water. Surprisingly, the d_h values were larger for the G_n-IPh-Glu and G_n-IPh-Gal series compared to those for G_n-IPh-OEG-Gal. A similar trend was observed for the corresponding glyco-DDM/DOX complexes. Both in water and PBS, the DDM/DOX complexes were much larger than the bare DDMs (20−80 nm in size, except for the G_3-IPh-Glu_{32}/DOX complex, which was much larger). The size of particles increased with the DDM generation. In PBS buffer, the particles possessed slightly larger diameters. Contrarily, the size of the G_n-IPh-Gal series decreased with the generation (from ≈86 nm for G_1 to ≈5 nm for G_3). Zeta potential (ξ) measurements revealed that, in most cases, the glyco-DDMs and glyco-DDM/DOX complexes possessed negative values, and ξ-values of the complexes were slightly lower compared to those of bare DDMs.

It was shown before that glyco-DDMs possess small d_h (≈0.5 to 3.6 nm) depending on the generation and surface modification.[42,74,75] Similar dimensions of isolated DDMs studied in this work were obtained by analysis of their molecular models (Section 3.10). Larger d_h values indicate a tendency of these nanoparticles to assemble into more complex structures in water-based solvents. A spontaneous self-assembling process was enhanced after the DOX encapsulation, and as a result, we observed a significant increase in d_h, especially for the G_n-IPh-Glu series. Similar behavior was also observed for mPEGylated peptide DDM/DOX conjugates[76] and chimeric polypeptide−DOX conjugates.[77] The aggregation tendency was explained by the minimization of the interfacial energy governed by the balance between the hydrophilic and hydrophobic character of the molecular structure. Glyco-DDMs were constructed similarly since they possess a hydrophobic carbosilane interior surrounded by hydrophilic glyco- or glyco-OEG moieties. We may therefore hypothesize that the DOX encapsulation could disturb the stability of the dendritic aggregates resulting in the formation of larger nanoparticle structures via the self-assembling process.

3.5. Fluorescence Spectra and Intensity of Glyco-DDM/DOX Complexes. Excitation and emission spectra were measured for DOX and glyco-DDM/DOX complexes (Figure S5). The emission spectrum of DOX has two maxima peaks located at 555/590 nm. The intensity of the first maxima peak (I^{1st}) is much lower than that of the second (I^{2nd}) with ca. 13% difference. Emission spectra of all glyco-DDM/DOX complexes were similar to each other as well as to those of pure DOX. Generally, compared to DOX, the position of the I^{1st} was shifted in all complexes to longer wavelengths by 1−3 nm depending on the DDM type and generation (Table S4), although no general reliance on the DDM type or generation was observed. The I^{2nd} position was shifted to shorter wavelengths, and the differences between control (DOX) and complexes were within 1−5 nm. Similarly, there was no reliance on the DDM type or generation. Apart from the maxima peak shifts, changes in relative intensities of both peaks were also observed in glyco-DDM/DOX complexes. While for the pure DOX, the I^{1st}/I^{2nd} ratio is 0.87, for all glyco-DDM/DOX complexes, the I^{1st}/I^{2nd} ratio was higher than 0.92. Usually, when the fluorophore is in a more hydrophobic environment, there is a significant peak at 630 nm. However, in our case, a long-wavelength shoulder of DOX positioned near 630 nm remained unchanged irrespectively of DOX encapsulation. Also, there were no differences in the excitation spectrum positions between pure DOX and the complexes.

It is evident that the differences in the positions of the fluorescence maxima and relative fluorescence intensities observed between the pure DOX (control sample) and glyco-DDM/DOX complexes can be related to the encapsulation process. Commonly, the changes in the polarity of fluorophore surroundings can substantially affect the maxima positions and/or intensities of fluorescence.[78] With our complexes, it seems plausible to assume that DOX interacts with the glyco-DDMs preferentially through the hydrophobic interactions (nonpolar carbosilane interior). This leads to the prediction that the environment polarity in which the DOX molecules are found after encapsulation into the glyco-DDMs is very different from the environment of pure DOX dissolved in water. Such a change in the environment polarity may cause a shift of the emission fluorescence maxima to a shorter wavelength, as was observed for some fluorophores.[78,79] Moreover, the change in the polarity of the DOX environment also influences the shape of the emission spectra by leveling the two maxima. It was shown that the intensity difference between the I^{1st} and I^{2nd} was decreasing due to hydrophobic interactions. In some cases, the I^{1st} had a higher value than the I^{2nd}.[79,80] Since the observed changes of the DDM/DOX complexes fluorescence were only moderate (considering no evident changes of the 630 nm peak), it seems reasonable to assume that the DOX encapsulation carries out in the interphase between the hydrophilic glyco-functionalized surface and hydrophobic DDM interior. Optical properties of DOX located in the interphase between the hydrophobic and

https://doi.org/10.1021/acs.biomac.1c01264
Biomacromolecules 2022, 23, 276−290

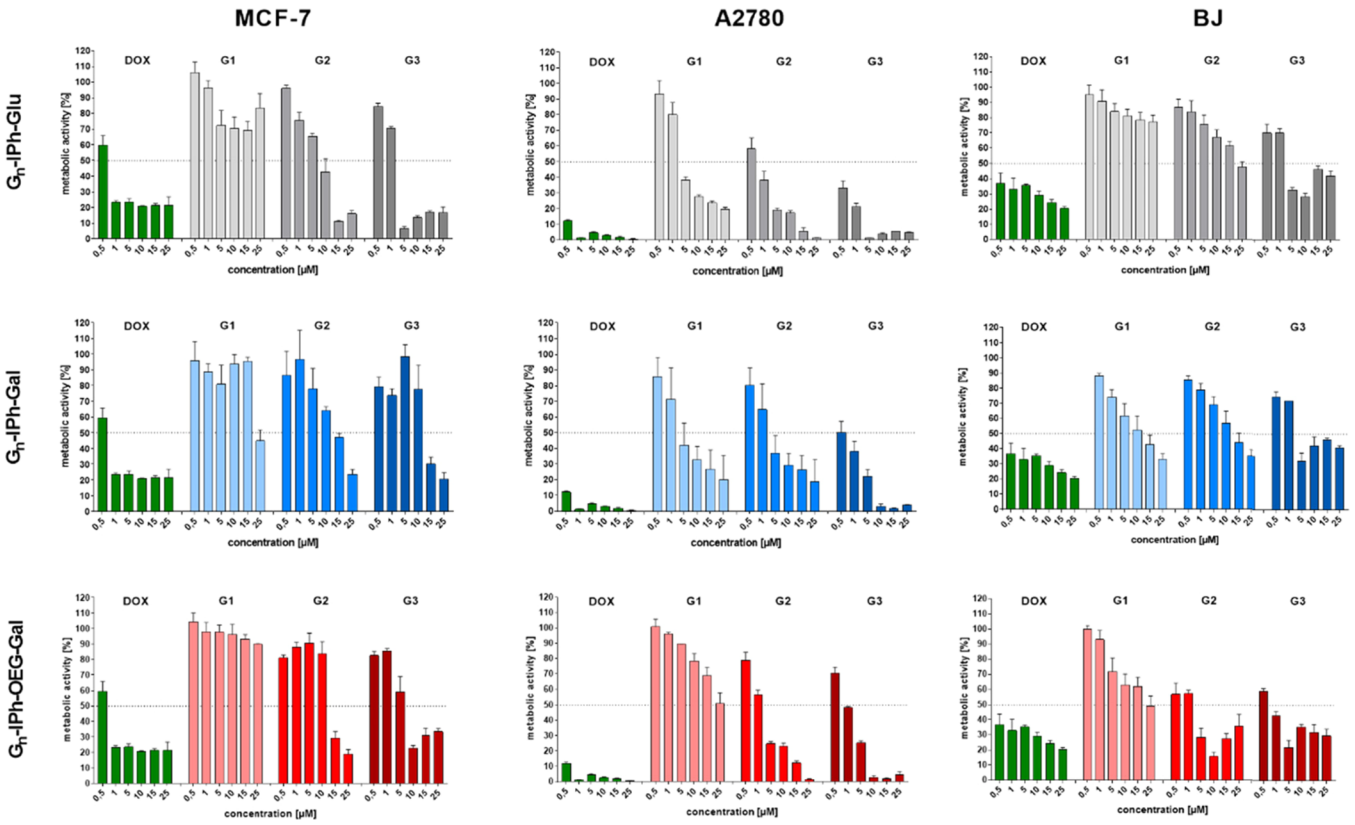

Figure 2. In vitro cell viability of cancer (MCF-7, A2780) and normal (BJ) cell lines after treatment with free DOX and glyco-DDM/DOX complexes (G_n-IPh-Glu/DOX, G_n-IPh-Gal/DOX, and G_n-IPh-OEG-Gal/DOX) at different concentrations of encapsulated DOX (0.5−25 μM range). Untreated MCF-7, A2780, and BJ cells were used as a control.

hydrophilic areas of the glyco-DDMs may exhibit some features typical for both nonpolar and polar environments. Moreover, the DOX position in the interphase may be stabilized by two types of interactions: (i) hydrogen bonding between the DOX aminoglycosidic side chain and the saccharide moieties of the DDMs; (ii) hydrophobic interactions of the anthraquinone ring system with the DDM interior.[79]

3.6. Cytotoxicity of Glyco-DDM/DOX Complexes. The IC_{50} values revealed differences in the cytotoxicity of the glyco-DDM/DOX series (Table 2). In the case of G_n-IPh-Glu/DOX, the cytotoxicity toward cancer cell lines (MCF-7 and A2780) is considerably higher than that toward the noncancer cell line (BJ). The high toxicity is notably pronounced for the A2780 cell line (Figure 2). G_1-IPh-Glu/DOX showed an IC_{50} value of 58.3 μM for noncancer BJ cells and 4.0 μM for A2780 cancer cells. Moreover, in general, the glyco-DDMs were significantly more toxic to A2780 cells. Considering G_n-IPh-Glu/DOX, the G_n-IPh-Gal/DOX series is comparably toxic toward both cancer cell lines; however, it is also moderately toxic to the normal cell line. In G_n-IPh-OEG-Gal/DOX, we introduced OEG chains into the DDM structure to investigate an influence on the cytotoxicity of the complexes. To our surprise, the presence of OEG linkers in the DDM structure has no significant additional influence on the viability of both cancer and noncancer cells.

Generally, the cytotoxicity of the glyco-DDM/DOX complex raises with increasing DDM generation. While generally showing certain selectivity toward cancer cell lines, the glyco-DDM/DOX complexes are much more selective to A2780 cells than the MCF-7 cell line (IC_{50} values are roughly 5−6 times lower). It is evident that the presence of peripheral saccharide moieties fundamentally decreases the cytotoxicity of the glyco-DDM/DOX complexes. As a result, a higher amount of DOX can be introduced in cancer therapy while simultaneously reducing the toxic effect of DOX due to the presence of a remarkably biocompatible glyco-DDM transporter, which is in accordance with some other glyco-DDM-based nanonocarriers.[33,37,81] Performance of the G_1 glyco-DDM/DOX complexes generally differs from the higher generations; despite being the smallest in size (and bearing the lowest number of saccharide moieties), they show roughly 3−10 times lower cytotoxicity compared to the free DOX in the same absolute concentration. This behavior is even more surprising because the G_1 glyco-DDMs encapsulate a comparable number of DOX molecules to G_2 and G_3. In addition, in some absolute concentrations of DOX, the G_2 and G_3 glyco-DDM/DOX complexes are more toxic than free DOX. Slightly higher toxicity of the DOX conjugate compared to free DOX was reported in the PAMAM-based PEGylated nanocarrier modified with transferrin and wheat germ agglutinin (C6 glioma and BMWEC cells)[39] and in dextran-conjugated PPI-based dendritic vectors (A549 cells).[34] With increasing concentration (10−25 μM) of our complexes, the cell viability steeply decreases, revealing the ability of the G_2 and G_3 glyco-DDM/DOX (IC_{50} of 13.2−2.8 μM) to inhibit MCF-7 cancer cells. In addition to this, the glyco-DDM/DOX complexes show significant toxicity against the A2780 cancer cells even at lower concentrations (from 5 μM; IC_{50} values 3.1−0.3 μM on average). Regarding this, we may generally

https://doi.org/10.1021/acs.biomac.1c01264
Biomacromolecules 2022, 23, 276−290

consider G_2 and G_3 glyco-DDM/DOX complexes effective against MCF-7 and A2780 cancer cell lines.

3.7. Hematotoxicity of the Glyco-DDM/DOX Complexes. The cyanmethemoglobin test revealed low hemolysis levels (5−9%) after exposure of human blood samples to glyco-DDM/DOX complexes, which follows published data for other DDM-based nanocarriers.[37,81] In both tested concentrations, the glyco-DDM/DOX complexes (IC_{50} concentration, 25 μM) showed lower hematotoxicity than free DOX (Figure 3; Table S3). There is a negligible difference in hemolysis levels induced by particular glyco-DDM series suggesting no significant impact of either OEG chains or saccharide stereo configuration on hematotoxicity. In addition, minor distinction of hemolytic toxicity between glyco-DDM generations with no particular trend was observed.

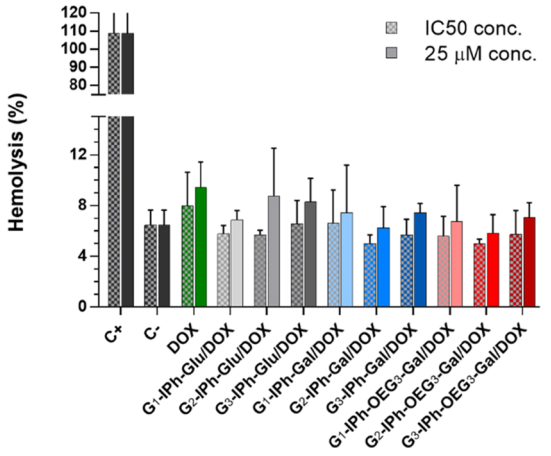

Figure 3. Hematolysis levels after exposure to pure DOX and glyco-DDM/DOX complexes at IC_{50} and 25 μM concentration. As controls, dH_2O (C+) and PBS solution (C−) were used.

3.8. DOX Release Assay. Physiological and acidic (pH 5.0) PBS solutions simulated environments of blood and other body fluids (pH 7.4), tumors (pH ∼ 6.5), and endo/lysosomes (pH 5.0−6.0)[82] during the drug release. The majority of DOX was generally released within 24−48 h (Figure 4; for 0−8 h detail, see Figure S4). Generally, cumulative release (CR) levels differ slightly with respect to the glyco-DDM/DOX series. However, the CR levels of 10−30% under physiological conditions and 18−50% in an acidic environment agree with the release rates reported for other dendritic DOX conjugates.[37,76] Under both physiological and acidic conditions, the CR of DOX decreased with increasing DDM generation. The reason behind this might be the looser architecture of lower generation DDMs that facilitates disengagement of DOX molecules from the complexes. Considering the pKa value of the 3′amino group of daunosamine in the DOX molecule (9.93),[83] we assume that the DOX molecule is prevalently protonated in pH 5.0, thus more hydrophilic, and prone to disengage the complex. However, this applies convincingly to the G_n-IPh-Glu series, where the CR of G_1, G_2, and G_3 after 24 h was by 27, 42, and 97% higher in acidic environments compared to physiological pH. The differences between CR of the G_n-IPh-Gal and G_n-IPh-OEG-Gal series based on pH are much less dramatic. Because OEG has been reported to improve the wettability and solubility of hydrophobic drugs, we assumed that the presence of OEG chains might ease the transfer of DOX from the hydrophobic interior to the release medium. Moreover, an increased DOX release was reported in partly PEGylated PAMAM transporters.[37] However, in the case of G_n-IPh-Gal and G_n-IPh-OEG-Gal series, only minor differences in CR values were observed. The rate of DOX release in glyco-DDM/DOX complexes can be attributed to the hindrance of sugar groups attached to the DDM, which hamper the diffusion of the drug to the medium.[84,85]

3.9. Confocal Fluorescence Microscopy Studies of Cellular Internalization and Localization of Glyco-DDM/DOX Complexes. Visualization of cellular internalization and localization of DOX and glyco-DDM/DOX complexes was investigated by confocal laser scanning fluorescence microscopy. Figures 5 and S6−S8 show images of DOX and glyco-DDM/DOX complex uptake by three human cell lines: MCF7, A2780, and BJ. Nuclei of all cells were stained with Hoechst 33342 (blue color). DOX and the glyco-DDM/DOX complexes were red due to the fluorescence properties of DOX. Microscopy observations of the cell treated with pure DOX revealed a strong fluorescence signal in the nucleus after 90 min of incubation. Contrarily, within the same period, the glyco-DDM/DOX complexes were transported to the cell interior and remained particularly in the cytoplasm (no red color signal from the nuclei in the samples was detected). Moreover, the noncancer cell line (BJ) did not uptake glyco-DDM/DOX complexes as easily as the cancer cell lines (MCF-7 and A2780).

For most cell types, 1−2 h of incubation should be sufficient for the DOX nuclear accumulation.[86−88] Differences in the

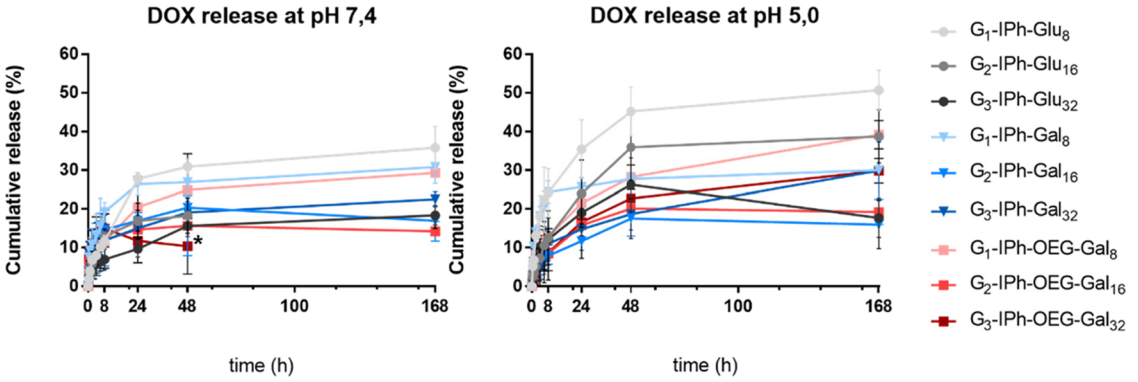

Figure 4. In vitro DOX release from glyco-DDM/DOX complexes in PBS solutions at pH of 7.4 (left) and 5.0 (right). *The CR peaked in less than 48 h.

https://doi.org/10.1021/acs.biomac.1c01264
Biomacromolecules 2022, 23, 276−290

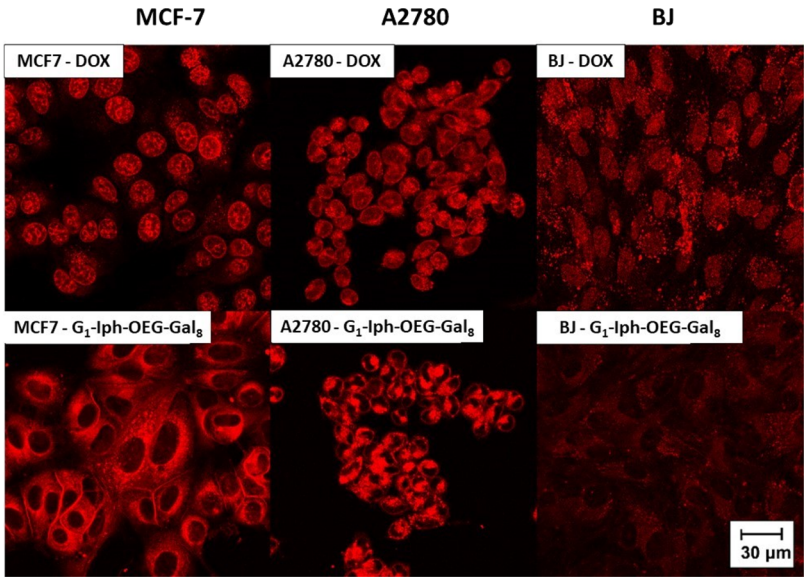

Figure 5. Representative confocal laser scanning fluorescence microscopy images of cellular internalization of DOX and G_1-IPh-OEG-Gal_8/DOX complexes in the three cell lines—MCF7, A2780, and BJ.

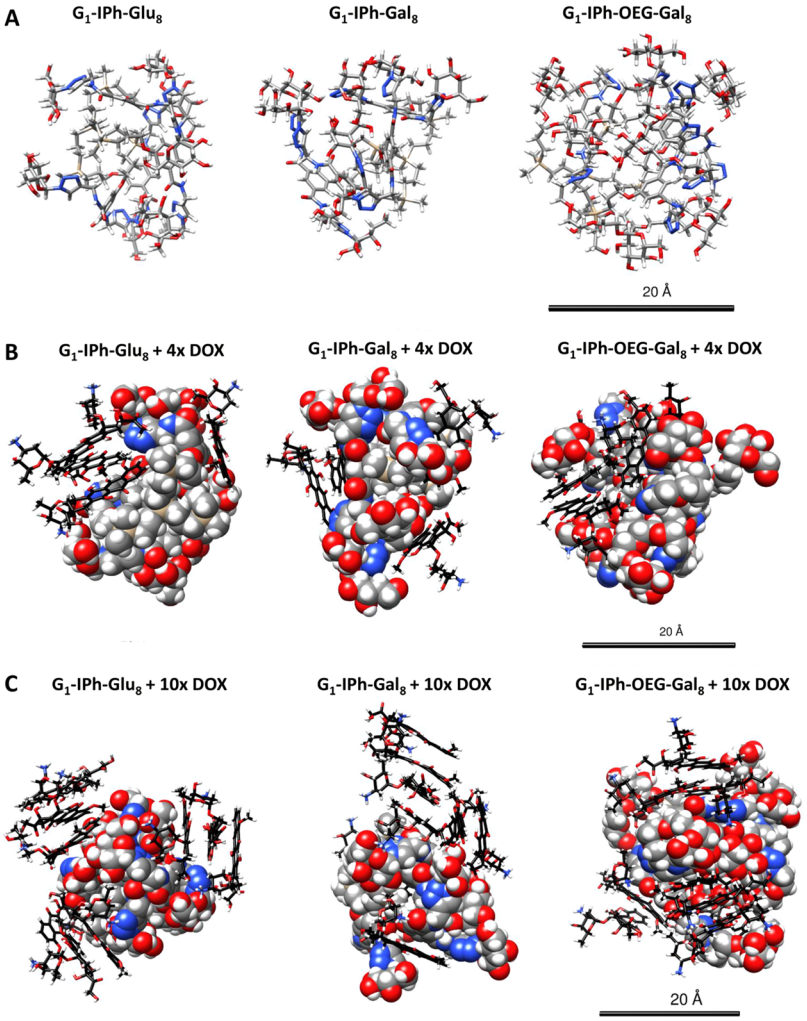

Figure 6. Computer models obtained by molecular dynamics simulation in explicit water. Colors: C—gray/black; O—red; H—white; Si—beige; N—blue. (A) G1 glyco-DDMs, (B) G_1 glyco-DDM/DOX complexes in a 1:4 molar ratio, (C) G_1 glyco-DDM/DOX complexes in a 1:10 molar ratio. DOX carbons are depicted in black for better clarity.

https://doi.org/10.1021/acs.biomac.1c01264
Biomacromolecules 2022, 23, 276−290

cellular uptake between pure DOX and drug delivery systems comprising DDM/DOX complexes and slower release kinetics of DOX with a delayed nuclear localization were already reported.[89−91] Moreover, DOX was more effectively delivered to the cancer cells, and the selectivity of the drug delivery was achieved via a suitable design of the drug delivery systems. The microscopy studies showed that (i) the glyco-DDM/DOX complexes were effectively transported to the cell interior, and (ii) the complexes were localized particularly in the cytoplasm during the relatively short incubation time. In accordance with the measured time scale of DOX release from the complexes, this may indicate that a longer time is needed for an effective DOX accumulation in nuclei. Just as pure DOX can quickly enter cells, it can also be quickly released. Inside the cells, DOX can be released from the glyco-DDM/DOX complexes gradually. As a result, DOX is present in cells for a longer period of time, inducing cell death. The concentration of DOX in the nucleus can be lower, and still, its interaction time can be prolonged. This clarifies the observed higher IC_{50} of the glyco-DDM/DOX complexes compared to pure DOX. Additional experiments to study the DOX release from the glyco-DDM/DOX complexes while being 24 h in the cells are planned beyond the scope of this publication.

Moreover, differences in cellular uptake efficiency were observed between individual types of the glyco-DDM/DOX complexes and the types of the cell lines. Cellular uptake was determined by the size of the glyco-DDM/DOX complexes, where the smaller complexes were internalized more easily. It was particularly evident in the case of G_n-IPh-OEG-Gal complexes. A substantial difference in the cellular uptake was observed between cancer cell lines (MCF-7 and A2780) and the noncancer cell line (BJ). The glyco-DDM/DOX complexes were much less internalized in BJ compared to both cancer cell lines. This partially agrees with the observed differences in toxicity of the glyco-DDMs and glyco-DDM/DOX complexes toward cancer and noncancer cell lines discussed in Sections 3.2 and 3.6. Although the preferential cancer cell internalization of the glyco-DDM/DOX complexes was demonstrated, a more thorough investigation of the cellular uptake mechanism and DOX release kinetics should be conducted. Such research was out of the scope of this paper.

3.10. Computer Modeling of Glyco-DDMs and Glyco-DDM/DOX Complexes. Glyco-DDMs and their interaction with DOX was studied using molecular dynamics in explicit water. Simulated computer models of the G_1 glyco-DDMs are shown in Figure 6A (for higher generations, see Figures S9A and S10A). The size of the glyco-DDMs increases with increasing generation; yet, it is almost independent of the DDM type (Table 3). Thus, the short OEG linkers in G_n-IPh-OEG-Gal series do not seem to affect the size of the glyco-DDMs significantly.

Additionally, interactions of the glyco-DDMs with DOX molecules were simulated in two different DOX/DDM molar ratios: (i) 10:1, corresponding to the ratio used in the encapsulation experiments, and (ii) 4:1, making it easier to study interactions of individual DOX molecules (not DOX clusters) with the glyco-DDMs. The computer simulations revealed a strong tendency of DOX molecules to bind to the glyco-DDMs (Figures 6B,C, S9B,C, and S10B,C). This tendency comes mainly from the rather hydrophobic nature of DOX. In this case, mutual aggregation or association with other molecules is energetically favorable for the whole system as the contact of these molecules with a strongly polar solvent is reduced. Regardless of series and generation, the glyco-DDMs could bind all DOX molecules present in the simulated systems, i.e., 4 or 10 DOX molecules.

Table 3. Size Characteristics of Solvated Glyco-DDM Models[a]

R_g [Å]	G_n-IPh-Glu	G_n-IPh-Gal	G_n-IPh-OEG-Gal
G_1	8.48 ± 0.20	8.44 ± 0.20	9.28 ± 0.26
G_2	10.86 ± 0.12	10.85 ± 0.11	11.76 ± 0.20
G_3-	14.79 ± 0.12	15.18 ± 0.12	15.18 ± 0.13
R_{max} [Å]			
G_1	14.33 ± 1.17	12.70 ± 1.50	15.35 ± 3.04
G_2	18.07 ± 1.76	18.00 ± 2.03	19.97 ± 1.59
G_3-	22.42 ± 3.65	25.90 ± 0.70	26.92 ± 1.57

[a] R_g—radius of gyration; R_{max}—maximal distance between the glyco-DDM atoms and the glyco-DDM center of mass (their estimated radius for spherical molecules). Data obtained from analysis of the last 20 ns of the simulation trajectories (150 ns in total) are presented as average values ± SD.

Even the G_1 glyco-DDMs were able to bind 10 DOX molecules. It can be explained by the tendency of the DOX molecules to form clusters in water (depending on concentration). Therefore, small glyco-DDMs serve as a support for the formation of these clusters or simply as their binding molecular partner. In such a case, it is obvious that more DOX molecules can be associated with the DDM than in the case of exclusively single-molecular DDM−DOX interactions. Thus, even the smallest DDMs are able to bind a relatively high number of DOX molecules. The DOX molecules were able to interact both with the hydrophilic parts of the glyco-DDMs (saccharides), where the mutual interaction was supported by hydrogen bonds and with the internal hydrophobic CS structure. These findings are in accordance with our experimental results except for the DDM binding capacity. In the case of the 10:1 DOX/DDM molar ratio (i.e., the ratio used in the experiments), the DDM binding capacity is higher in simulations than in experiments due to about 100 times higher absolute concentration of molecules. Moreover, in the experiments, supramolecular glyco-DDM/DOX complexes (i.e., consisting of more DDMs) are formed as follows from DLS analyses. In addition, the interactions of DOX molecules occurred mainly on the surface of the glyco-DDMs, relatively independently of the local nature (hydrophilic/hydrophobic). However, partial penetration of DOX molecules between the DDM surface groups was observed (Figures 6C, S9B,C, S10B,C, and S11). As was stated earlier, in the real environment, supramolecular glyco-DDM/DOX clusters are formed. Thus, in addition to surface interactions of DOX and the glyco-DDMs, some portion of DOX molecules is probably trapped within the supramolecular clusters. Binding energies (ΔG) between DOX molecules and the glyco-DDMs were calculated using the MM/PBSA method. Irrespective of the glyco-DDM type and generation, the ΔG values of the surface-bound DOX molecules were mainly in the range of −30 to −20 kcal/mol. Binding to the glyco-DDM surface was stronger in the case of DOX dimers or trimers (−70 to −35 kcal/mol), as well as in the case of individual DOX molecules that penetrated deeper into the glyco-DDM structure (−50 to −40 kcal/mol; Figures 7 and S11).

Beyond this, in the case of the third generation, the ability of dendrimers to form 1 + 1 complexes in the pure water as well

https://doi.org/10.1021/acs.biomac.1c01264
Biomacromolecules 2022, 23, 276−290

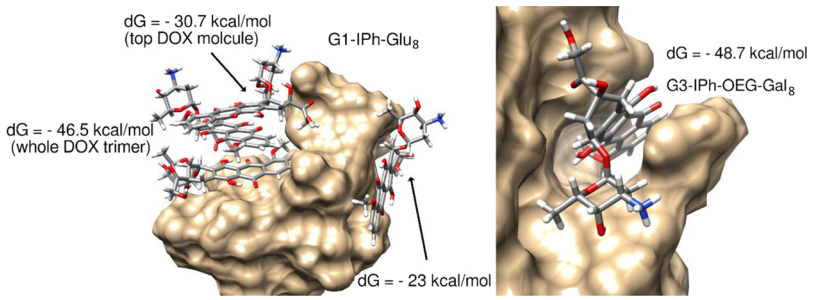

Figure 7. Illustration of several possible interaction modes and calculated binding energies related to glyco-DDM/DOX complexes (molar ratio 4:1). The glyco-DDM molecular surface was visualized, and DOX carbons are depicted black for better clarity.

as in the presence of DOX was confirmed using molecular simulations. Further details (i.e., analysis and comparison of the resulting complexes) are provided in the Supporting Information (section: "Glyco-DDM/glyco-DDM/DOX interactions" and Figures S12−S15). In conclusion, under the given conditions, computer simulations demonstrated the ability of the glyco-DDMs to form DOX complexes and clusters in an aqueous environment.

4. CONCLUSIONS

We developed a robust synthetic procedure for the preparation of alkyne-terminated CS-DDMs enabling further peripheral derivatization with a plethora of functional moieties. A series of water-soluble glyco-DDMs with peripheral glucose, galactose, and oligo (ethylene glycol) modified galactose units was synthesized using this methodology.

Regardless of the DDM series and generation, the compounds exhibited outstanding biocompatibility with all tested cell lines indicating their potential as nanocarriers in drug delivery. Upon DOX encapsulation, stable glyco-DDM/DOX complexes were formed, showing similar entrapment capacity (4−6 DOX molecules per one DDM) across the DDM series and generations.

The fluorescent microscopy suggested that the DOX molecules in the complexes are located in the interphase between the saccharide-modified periphery and hydrophobic carbosilane interior. In support of these findings, computer simulations showed DOX interactions with both hydrophilic and hydrophobic glyco-DDM domains implying their essential role in the encapsulation process. In vitro cytotoxicity assay of the glyco-DDM/DOX complexes revealed generation and concentration-dependent effects across cell lines. Yet, the complexes showed general selectivity toward cancer cell lines, being 5−6 times more selective to the A2780 cell line compared to the MCF-7 cell line. Higher IC_{50} values of the majority of the complexes compared to pure DOX showed that the peripheral saccharide units substantially decreased the cytotoxicity of the glyco-DDM/DOX complexes. Thus, for the benefit of cancer therapy, higher dose of DOX can be introduced using the glyco-DDM nanocarriers, whereas slower drug release stabilizes the concentration of the therapeutic agent in cancer cells. In addition, the DOX release was up to 2−3 times faster in acidic environments than under physiological conditions (pH 7.4), indicating preferential drug release in the vicinity of tumor tissues. A substantial difference in the cellular uptake was observed: the glyco-DDM/DOX complexes were much less internalized in noncancerous BJ cells compared to both cancerous cell lines. Still, further in-depth research into the cellular uptake mechanisms and trans-barrier trafficking is called for before these systems being tested in vivo. To the best of our knowledge, this is the first systematic study of CS glyco-DDM-based drug delivery systems having prospects for a wide range of bioapplications.

■ ASSOCIATED CONTENT

Supporting Information

The Supporting Information is available free of charge at https://pubs.acs.org/doi/10.1021/acs.biomac.1c01264.

Additional experimental details including synthesis and characterization, data, and spectra (PDF)

■ AUTHOR INFORMATION

Corresponding Authors

João Rodrigues − *CQM-Centro de Química da Madeira, Universidade da Madeira, 9020-105 Funchal, Portugal*; Email: joaoc@staff.uma.pt

Tomáš Strašák − *The Czech Academy of Sciences, Institute of Chemical Process Fundamentals, 165 02 Prague, Czech Republic; Faculty of Science, University of Jan Evangelista Purkyně in Ústí nad Labem, 400 96 Ústí nad Labem, Czech Republic*; orcid.org/0000-0001-6413-0494; Email: strasak@icpf.cas.cz

Authors

Monika Müllerová − *The Czech Academy of Sciences, Institute of Chemical Process Fundamentals, 165 02 Prague, Czech Republic; Faculty of Science, University of Jan Evangelista Purkyně in Ústí nad Labem, 400 96 Ústí nad Labem, Czech Republic*

Dina Maciel − *CQM-Centro de Química da Madeira, Universidade da Madeira, 9020-105 Funchal, Portugal*

Nádia Nunes − *CQM-Centro de Química da Madeira, Universidade da Madeira, 9020-105 Funchal, Portugal*

Dominika Wrobel − *Faculty of Science, University of Jan Evangelista Purkyně in Ústí nad Labem, 400 96 Ústí nad Labem, Czech Republic*

Marcel Stofik − *Faculty of Science, University of Jan Evangelista Purkyně in Ústí nad Labem, 400 96 Ústí nad Labem, Czech Republic*

Lucie Červenková Šťastná − *The Czech Academy of Sciences, Institute of Chemical Process Fundamentals, 165 02 Prague, Czech Republic; Faculty of Science, University of Jan Evangelista Purkyně in Ústí nad Labem, 400 96 Ústí nad Labem, Czech Republic*

Alena Krupková − *The Czech Academy of Sciences, Institute of Chemical Process Fundamentals, 165 02 Prague, Czech Republic; Faculty of Science, University of Jan Evangelista*

https://doi.org/10.1021/acs.biomac.1c01264
Biomacromolecules 2022, 23, 276−290

Purkyně in Ústí nad Labem, 400 96 Ústí nad Labem, Czech Republic; orcid.org/0000-0001-9428-6393

Petra Cuřínová − *The Czech Academy of Sciences, Institute of Chemical Process Fundamentals, 165 02 Prague, Czech Republic; Faculty of Science, University of Jan Evangelista Purkyně in Ústí nad Labem, 400 96 Ústí nad Labem, Czech Republic*

Kateřina Nováková − *The Czech Academy of Sciences, Institute of Organic Chemistry and Biochemistry, 166 10 Prague, Czech Republic*

Matěj Božík − *Department of Food Science, Faculty of Agrobiology, Food and Natural Resources, Czech University of Life Sciences Prague, 16500 Praha-Suchdol, Czech Republic;* orcid.org/0000-0002-9020-8213

Marek Malý − *Faculty of Science, University of Jan Evangelista Purkyně in Ústí nad Labem, 400 96 Ústí nad Labem, Czech Republic*

Jan Malý − *Faculty of Science, University of Jan Evangelista Purkyně in Ústí nad Labem, 400 96 Ústí nad Labem, Czech Republic;* orcid.org/0000-0002-7022-2157

Complete contact information is available at: https://pubs.acs.org/10.1021/acs.biomac.1c01264

Notes

The authors declare no competing financial interest.

■ ACKNOWLEDGMENTS

The authors acknowledge the Czech Science Foundation project No. 20-21421S and assistance provided by the Research Infrastructure NanoEnviCz (Project No. LM2018124) and the project Pro-NanoEnviCz (Reg. No. CZ.02.1.01/0.0/0.0/16_013/0001821), supported by the Ministry of Education, Youth and Sports of the Czech Republic and the European Union—European Structural and Investments Funds in the frame of the Operational Programme Research Development and Education, the ERDF/ESF project "UniQSurf - Centre of biointerfaces and hybrid functional materials" (No. CZ.02.1.01/0.0/0.0/17_048/0007411), the project No. UJEP-IGA-TC-2019-53-01-2 and the project COST LTC19049 supported by the Ministry of Education, Youth and Sports of the Czech Republic. This work was also supported by FCT-Fundação para a Ciência e a Tecnologia, Portugal (Base Fund UIDB/00674/2020 and Programmatic Fund UIDP/00674/2020, Portuguese Government Funds), ARDITI—Agência Regional para o Desenvolvimento da Investigação Tecnologia e Inovação, through the project M1420-01-0145-FEDER-000005-CQM$^+$ (Madeira 14-20 Program), and the FCT Ph.D. Grant Ref. 2020.04679.BD (N.N.). This publication results from a joint work produced in the scope of COST Action CA 17140 "Cancer Nanomedicine from the Bench to the Bedside" supported by COST (European Cooperation in Science and Technology). The authors would like to thank Dr Vladimir Žegarac for proofreading the manuscript.

■ REFERENCES

(1) Jayaraman, N. Multivalent ligand presentation as a central concept to study intricate carbohydrate−protein interactions. *Chem. Soc. Rev.* **2009**, *38*, 3463−3483.

(2) Müller, C.; Despras, G.; Lindhorst, T. K. Organizing multivalency in carbohydrate recognition. *Chem. Soc. Rev.* **2016**, *45*, 3275−3302.

(3) Fasting, C.; Schalley, C. A.; Weber, M.; Seitz, O.; Hecht, S.; Koksch, B.; Dernedde, J.; Graf, C.; Knapp, E.-W.; Haag, R. Multivalency as a Chemical Organization and Action Principle. *Angew. Chem., Int. Ed.* **2012**, *51*, 10472−10498.

(4) Chabre, Y. M.; Roy, R. *Advances in Carbohydrate Chemistry and Biochemistry*; Academic Press, 2010; Vol. *63*, Chapter 6, pp. 165−393.

(5) Gao, J.; Ma, L.; Liu, D.; Wang, Z. Microarray-based technology for glycomics analysis. *Comb. Chem. High Throughput Screening* **2012**, *15*, 90−99.

(6) Gemeiner, P.; Mislovičová, D.; Tkáč, J.; Švitel, J.; Pätoprstý, V.; Hrabárová, E.; Kogan, G.; Kožár, T. Lectinomics: II. A highway to biomedical/clinical diagnostics. *Biotechnol. Adv.* **2009**, *27*, 1−15.

(7) Arnaud, J.; Audfray, A.; Imberty, A. Binding sugars: from natural lectins to synthetic receptors and engineered neolectins. *Chem. Soc. Rev.* **2013**, *42*, 4798−4813.

(8) Jiménez Blanco, J. L.; Ortiz Mellet, C.; García Fernández, J. M. Multivalency in heterogeneous glycoenvironments: hetero-glycoclusters, −glycopolymers and -glycoassemblies. *Chem. Soc. Rev.* **2013**, *42*, 4518−4531.

(9) Bojarová, P.; Křen, V. Sugared biomaterial binding lectins: Achievements and perspectives. *Biomater. Sci.* **2016**, *4*, 1142−1160.

(10) Jebali, A.; Nayeri, E. K.; Roohana, S.; Aghaei, S.; Ghaffari, M.; Daliri, K.; Fuente, G. Nano-carbohydrates: Synthesis and application in genetics, biotechnology, and medicine. *Adv. Colloid Interface Sci.* **2017**, *240*, 1−14.

(11) Pieters, R. J. Toward multivalent carbohydrate drugs. *Drug Discov. Today Technol.* **2009**, *6*, e27−e31.

(12) Chabre, Y. M.; Roy, R. Multivalent glycoconjugate syntheses and applications using aromatic scaffolds. *Chem. Soc. Rev.* **2013**, *42*, 4657−4708.

(13) Duan, Z.; Luo, Q.; Dai, X.; Li, X.; Gu, L.; Zhu, H.; Tian, X.; Zhang, H.; Gong, Q.; Gu, Z.; Luo, K. Synergistic Therapy of a Naturally Inspired Glycopolymer-Based Biomimetic Nanomedicine Harnessing Tumor Genomic Instability. *Adv. Mater.* **2021**, *33*, No. 2104594.

(14) Cai, H.; Xiang, Y.; Zeng, Y.; Li, Z.; Zheng, X.; Luo, Q.; Zhu, H.; Gong, Q.; Gu, Z.; Liu, Y.; Zhang, H.; Luo, K. Cathepsin B-responsive and gadolinium-labeled branched glycopolymer-PTX conjugate-derived nanotheranostics for cancer treatment. *Acta Pharm. Sin. B* **2021**, *11*, 544−559.

(15) Jayaraman, N.; Nepogodiev, S. A.; Stoddart, J. F. Synthetic Carbohydrate-Containing Dendrimers. *Eur. J. Chem.* **1997**, *3*, 1193−1199.

(16) Percec, V.; Leowanawat, P.; Sun, H.-J.; Kulikov, O.; Nusbaum, C. D.; Tran, T. M.; Bertin, A.; Wilson, D. A.; Peterca, M.; Zhang, S.; Kamat, N. P.; Vargo, K.; Moock, D.; Johnston, E. D.; Hammer, D. A.; Pochan, D. J.; Chen, Y.; Chabre, Y. M.; Shiao, T. C.; Bergeron-Brlek, M.; André, S.; Roy, R.; Gabius, H.-J.; Heiney, P. A. Modular Synthesis of Amphiphilic Janus Glycodendrimers and Their Self-Assembly into Glycodendrimersomes and Other Complex Architectures with Bioactivity to Biomedically Relevant Lectins. *J. Am. Chem. Soc.* **2013**, *135*, 9055−9077.

(17) Yuan, H.; Luo, K.; Lai, Y.; Pu, Y.; He, B.; Wang, G.; Wu, Y.; Gu, Z. A Novel Poly(l-glutamic acid) Dendrimer Based Drug Delivery System with Both pH-Sensitive and Targeting Functions. *Mol. Pharmaceutics* **2010**, *7*, 953−962.

(18) Gu, Z.; Luo, K.; She, W.; Wu, Y.; He, B. New-generation biomedical materials: Peptide dendrimers and their application in biomedicine. *Sci. China Chem.* **2010**, *53*, 458−478.

(19) Appelhans, D.; Klajnert-Maculewicz, B.; Janaszewska, A.; Lazniewska, J.; Voit, B. Dendritic glycopolymers based on dendritic polyamine scaffolds: view on their synthetic approaches, characteristics and potential for biomedical applications. *Chem. Soc. Rev.* **2015**, *44*, 3968−3996.

(20) Gorzkiewicz, M.; Sztandera, K.; Jatczak-Pawlik, I.; Zinke, R.; Appelhans, D.; Klajnert-Maculewicz, B.; Pulaski, Ł. Terminal Sugar Moiety Determines Immunomodulatory Properties of Poly(propyleneimine) Glycodendrimers. *Biomacromolecules* **2018**, *19*, 1562−1572.

(21) Firdaus, S.; Geisler, M.; Friedel, P.; Banerjee, S.; Appelhans, D.; Voit, B.; Lederer, A. Glyco-pseudodendrimers on a Polyester Basis: Synthesis and Investigation of Protein−Pseudodendrimer Interaction. *Macromol. Rapid Commun.* **2018**, *39*, No. e1800364.
(22) Abbassi, L.; Chabre, Y. M.; Kottari, N.; Arnold, A. A.; André, S.; Josserand, J.; Gabius, H.-J.; Roy, R. Multifaceted glycodendrimers with programmable bioactivity through convergent, divergent, and accelerated approaches using polyfunctional cyclotriphosphazenes. *Polym. Chem.* **2015**, *6*, 7666−7683.
(23) Hatano, K.; Matsuoka, K.; Terunuma, D. Carbosilane glycodendrimers. *Chem. Soc. Rev.* **2013**, *42*, 4574−4598.
(24) Bagul, R. S.; Hosseini, M.; Shiao, T. C.; Saadeh, N. K.; Roy, R. Heterolayered hybrid dendrimers with optimized sugar head groups for enhancing carbohydrate-protein interactions. *Polym. Chem.* **2017**, *8*, 5354−5366.
(25) Patra, J. K.; Das, G.; Fraceto, L. F.; Campos, E. V. R.; Rodriguez-Torres, M. D. P.; Acosta-Torres, L. S.; Diaz-Torres, L. A.; Grillo, R.; Swamy, M. K.; Sharma, S.; Habtemariam, S.; Shin, H.-S. Nano based drug delivery systems: recent developments and future prospects. *J. Nanobiotechnol.* **2018**, *16*, 71.
(26) Medina, S. H.; el-Sayed, M. E. H. Dendrimers as carriers for delivery of chemotherapeutic agents. *Chem. Rev.* **2009**, *109*, 3141−3157.
(27) Shi, Y.; van der Meel, R.; Chen, X.; Lammers, T. The EPR effect and beyond: Strategies to improve tumor targeting and cancer nanomedicine treatment efficacy. *Theranostics* **2020**, *10*, 7921−7924.
(28) Foroozandeh, P.; Aziz, A. A. Insight into Cellular Uptake and Intracellular Trafficking of Nanoparticles. *Nanoscale Res. Lett.* **2018**, *13*, 339−339.
(29) Minotti, G.; Menna, P.; Salvatorelli, E.; Cairo, G.; Gianni, L. Anthracyclines: Molecular Advances and Pharmacologic Developments in Antitumor Activity and Cardiotoxicity. *Pharmacol. Rev.* **2004**, *56*, 185−229.
(30) Tacar, O.; Sriamornsak, P.; Dass, C. R. Doxorubicin: an update on anticancer molecular action, toxicity and novel drug delivery systems. *J. Pharm. Pharmacol.* **2013**, *65*, 157−170.
(31) Carvalho, C.; Santos, R.; Cardoso, S.; Correia, S.; Oliveira, P.; Santos, M.; Moreira, P. Doxorubicin: The Good, the Bad and the Ugly Effect. *Curr. Med. Chem.* **2009**, *16*, 3267−3285.
(32) Pugazhendhi, A.; Edison, T. N. J. I.; Velmurugan, B. K.; Jacob, J. A.; Karuppusamy, I. Toxicity of Doxorubicin (Dox) to different experimental organ systems. *Life Sci.* **2018**, *200*, 26−30.
(33) Xu, X.; Li, J.; Han, S.; Tao, C.; Fang, L.; Sun, Y.; Zhu, J.; Liang, Z.; Li, F. A novel doxorubicin loaded folic acid conjugated PAMAM modified with borneol, a nature dual-functional product of reducing PAMAM toxicity and boosting BBB penetration. *Eur. J. Pharm. Sci.* **2016**, *88*, 178−190.
(34) Agarwal, A.; Gupta, U.; Asthana, A.; Jain, N. K. Dextran conjugated dendritic nanoconstructs as potential vectors for anticancer agent. *Biomaterials* **2009**, *30*, 3588−3596.
(35) Zhang, Z.; Zhou, Y.; Zhou, Z.; Piao, Y.; Kalva, N.; Liu, X.; Tang, J.; Shen, Y. Synthesis of enzyme-responsive phosphoramidate dendrimers for cancer drug delivery. *Polym. Chem.* **2018**, *9*, 438−449.
(36) al-Jamal, K. T.; al-Jamal, W.'. T.; Wang, J. T. W.; Rubio, N.; Buddle, J.; Gathercole, D.; Zloh, M.; Kostarelos, K. Cationic Poly-l-lysine Dendrimer Complexes Doxorubicin and Delays Tumor Growth in Vitro and in Vivo. *ACS Nano* **2013**, *7*, 1905−1917.
(37) Zhu, S.; Hong, M.; Tang, G.; Qian, L.; Lin, J.; Jiang, Y.; Pei, Y. Partly PEGylated polyamidoamine dendrimer for tumor-selective targeting of doxorubicin: The effects of PEGylation degree and drug conjugation style. *Biomaterials* **2010**, *31*, 1360−1371.
(38) Han, L.; Huang, R.; Li, J.; Liu, S.; Huang, S.; Jiang, C. Plasmid pORF-hTRAIL and doxorubicin co-delivery targeting to tumor using peptide-conjugated polyamidoamine dendrimer. *Biomaterials* **2011**, *32*, 1242−1252.
(39) He, H.; Li, Y.; Jia, X.-R.; Du, J.; Ying, X.; Lu, W.-L.; Lou, J.-N.; Wei, Y. PEGylated Poly(amidoamine) dendrimer-based dual-targeting carrier for treating brain tumors. *Biomaterials* **2011**, *32*, 478−487.
(40) Strik, H. M.; Hoffmann, A. *Galectins*; John Wiley & Sons, 2008; Chapter 11, pp. 223−234.
(41) Bernardes, G. J. L.; Kikkeri, R.; Maglinao, M.; Laurino, P.; Collot, M.; Hong, S. Y.; Lepenies, B.; Seeberger, P. H. Design, synthesis and biological evaluation of carbohydrate-functionalized cyclodextrins and liposomes for hepatocyte-specific targeting. *Org. Biomol. Chem.* **2010**, *8*, 4987−4996.
(42) Liegertová, M.; Wrobel, D.; Herma, R.; Müllerová, M.; Šťastná, L. Č.; Cuřínová, P.; Strašák, T.; Malý, M.; Čermák, J.; Smejkal, J.; Štofik, M.; Maly, J. Evaluation of toxicological and teratogenic effects of carbosilane glucose glycodendrimers in zebrafish embryos and model rodent cell lines. *Nanotoxicology* **2018**, *12*, 797−818.
(43) Jain, K.; Kesharwani, P.; Gupta, U.; Jain, N. K. Dendrimer toxicity: Let's meet the challenge. *Int. J. Pharm.* **2010**, *394*, 122−142.
(44) van der Made, A. W.; van Leeuwen, P. W. N. M.; de Wilde, J. C.; Brandes, R. A. C. Dendrimeric silanes. *Adv. Mater.* **1993**, *5*, 466−468.
(45) Herma, R.; Wrobel, D.; Liegertová, M.; Müllerová, M.; Strašák, T.; Maly, M.; Semerádtová, A.; Štofik, M.; Appelhans, D.; Maly, J. Carbosilane dendrimers with phosphonium terminal groups are low toxic non-viral transfection vectors for siRNA cell delivery. *Int. J. Pharm.* **2019**, *562*, 51−65.
(46) Ochiai, H.; Uetake, Y.; Niwa, T.; Hosoya, T. Rhodium-Catalyzed Decarbonylative Borylation of Aromatic Thioesters for Facile Diversification of Aromatic Carboxylic Acids. *Angew. Chem., Int. Ed.* **2017**, *56*, 2482−2486.
(47) Kovac, P. *Carbohydrate Chemistry Proven Synthetic Methods*; Boca Raton: CRC Press, 2012; Vol. *1*, p. 468.
(48) Marchetti, P.; Jimenez Solomon, M. F.; Szekely, G.; Livingston, A. G. Molecular Separation with Organic Solvent Nanofiltration: A Critical Review. *Chem. Rev.* **2014**, *114*, 10735−10806.
(49) Wang, X.; Teng, Z.; Wang, H.; Wang, C.; Liu, Y.; Tang, Y.; Wu, J.; Sun, J.; Wang, H.; Wang, J.; Lu, G. Increasing the cytotoxicity of doxorubicin in breast cancer MCF-7 cells with multidrug resistance using a mesoporous silica nanoparticle drug delivery system. *Int. J. Clin. Exp. Pathol.* **2014**, *7*, 1337−1347.
(50) Modarresi, M.; Hajialyani, M.; Moasefi, N.; Ahmadi, F.; Hosseinzadeh, L. Evaluation of the Cytotoxic and Apoptogenic Effects of Glabridin and Its Effect on Cytotoxicity and Apoptosis Induced by Doxorubicin Toward Cancerous Cells. *Adv. Pharm. Bull.* **2019**, *9*, 481−489.
(51) Wang, J.; Wolf, R. M.; Caldwell, J. W.; Kollman, P. A.; Case, D. A. Development and testing of a general amber force field. *J. Comput. Chem.* **2004**, *25*, 1157−1174.
(52) Kirschner, K. N.; Yongye, A. B.; Tschampel, S. M.; González-Outeiriño, J.; Daniels, C. R.; Foley, B. L.; Woods, R. J. GLYCAM06: a generalizable biomolecular force field. Carbohydrates. *J. Comput. Chem.* **2008**, *29*, 622−655.
(53) Bayly, C. I.; Cieplak, P.; Cornell, W.; Kollman, P. A. A well-behaved electrostatic potential based method using charge restraints for deriving atomic charges: the RESP model. *J. Phys. Chem.* **1993**, *97*, 10269−10280.
(54) Götz, A. W.; Williamson, M. J.; Xu, D.; Poole, D.; Le Grand, S.; Walker, R. C. Routine Microsecond Molecular Dynamics Simulations with AMBER on GPUs. 1. Generalized Born. *J. Chem. Theory Comput.* **2012**, *8*, 1542−1555.
(55) Case, D. A., Brozell, S. R., Cerutti, D. S., Cheatham, T. E., III, Cruzeiro, V. W. D., Darden, T.A., Duke, R. E., Ghoreishi, D., Gohlke, H., Goetz, A. W., Greene, D., Harris, R., Homeyer, N., Izadi, S., Kovalenko, A., Lee, T. S., LeGrand, S., Li, P., Lin, C., Liu, J., Luchko, T., Luo, R., Mermelstein, D. J., Merz, K. M., Miao, Y., Monard, G., Nguyen, H., Omelyan, I., Onufriev, A., Pan, F., Qi, R., Roe, D. R., Roitberg, A., Sagui, C., Schott-Verdugo, S., Shen, J., Simmerling, C. J., Smith, J., Swails, J., Walker, R. C., Wang, J., Wei, H., Wolf, R. M., Wu, X., Xiao, L., York, D. M., Kollman, P. A. *AMBER 2018*; University of Carolina: San Francisco, 2018.
(56) Wang, E.; Sun, H.; Wang, J.; Wang, Z.; Liu, H.; Zhang, J. Z. H.; Hou, T. End-Point Binding Free Energy Calculation with MM/PBSA

https://doi.org/10.1021/acs.biomac.1c01264
Biomacromolecules 2022, 23, 276−290

and MM/GBSA: Strategies and Applications in Drug Design. *Chem. Rev.* **2019**, *119*, 9478−9508.
(57) Dupradeau, F.-Y.; Pigache, A.; Zaffran, T.; Savineau, C.; Lelong, R.; Grivel, N.; Lelong, D.; Rosanski, W.; Cieplak, P. The R.E.D. tools: advances in RESP and ESP charge derivation and force field library building. *Phys. Chem. Chem. Phys.* **2010**, *12*, 7821−7839.
(58) Schmidt, M. W.; Baldridge, K.; Boatz, J.; Elbert, S.; Gordon, M.; Jensen, J.; Koseki, S.; Matsunaga, N.; Nguyen, K.; Su, S.; Windus, T.; Dupuis, M.; Montgomery, J. General atomic and molecular electronic structure system. *J. Comput. Chem.* **1993**, *14*, 1347−1363.
(59) Gordon, M. S.; Schmidt, M. W. *Theory and Applications of Computational Chemistry*; Elsevier, 2005; Chapter 41, pp. 1167−1189.
(60) Lii, J.; Allinger, N. L. The MM3 force field for amides, polypeptides and proteins. *J. Comput. Chem.* **1991**, *12*, 186.
(61) Jorgensen, W. L.; Chandrasekhar, J.; Madura, J. D.; Impey, R. W.; Klein, M. L. Comparison of simple potential functions for simulating liquid water. *J. Chem. Phys.* **1983**, *79*, 926−935.
(62) Ryckaert, J.-P.; Ciccotti, G.; Berendsen, H. J. C. Numerical integration of the cartesian equations of motion of a system with constraints: molecular dynamics of n-alkanes. *J. Comput. Phys.* **1977**, *23*, 327−341.
(63) Wu, X.; Brooks, B. R.; Vanden-Eijnden, E. Self-guided Langevin dynamics via generalized Langevin equation. *J. Comput. Chem.* **2016**, *37*, 595−601.
(64) Roe, D. R.; Cheatham, T. E. PTRAJ and CPPTRAJ: Software for Processing and Analysis of Molecular Dynamics Trajectory Data. *J. Chem. Theory Comput.* **2013**, *9*, 3084−3095.
(65) Pettersen, E. F.; Goddard, T. D.; Huang, C. C.; Couch, G. S.; Greenblatt, D. M.; Meng, E. C.; Ferrin, T. E. UCSF Chimera–a visualization system for exploratory research and analysis. *J. Comput. Chem.* **2004**, *25*, 1605−1612.
(66) Miller, B. R.; McGee, T. D.; Swails, J. M.; Homeyer, N.; Gohlke, H.; Roitberg, A. E. MMPBSA.py: An Efficient Program for End-State Free Energy Calculations. *J. Chem. Theory Comput.* **2012**, *8*, 3314−3321.
(67) Baker, N. A.; Sept, D.; Joseph, S.; Holst, M. J.; McCammon, J. A. Electrostatics of nanosystems: Application to microtubules and the ribosome. *Proc. Natl. Acad. Sci. U. S. A.* **2001**, *98*, 10037−10041.
(68) Wrobel, D.; Müllerová, M.; Strašák, T.; Růžička, K.; Fulem, M.; Kubíková, R.; Bryszewska, M.; Klajnert-Maculewicz, B.; Malý, J. Glucose-modified carbosilane dendrimers: Interaction with model membranes and human serum albumin. *Int. J. Pharm.* **2020**, *579*, No. 119138.
(69) Meier, L.; Monteiro, G. C.; Baldissera, R. A. M.; Sá, M. M. Simple method for fast deprotection of nucleosides by triethylamine-catalyzed methanolysis of acetates in aqueous medium. *J. Braz. Chem. Soc.* **2010**, *21*, 859−866.
(70) Mishra, V.; Gupta, U.; Jain, N. K. Surface-Engineered Dendrimers: a Solution for Toxicity Issues. *J. Biomater. Sci. Polym. Ed.* **2009**, *20*, 141−166.
(71) Ortega, P.; Serramía, M. J.; Muñoz-Fernández, M. A.; Javier de la Mata, F.; Gómez, R. Globular carbosilane dendrimers with mannose groups at the periphery: synthesis, characterization and toxicity in dendritic cells. *Tetrahedron* **2010**, *66*, 3326−3331.
(72) Janaszewska, A.; Lazniewska, J.; Trzepiński, P.; Marcinkowska, M.; Klajnert-Maculewicz, B. Cytotoxicity of Dendrimers. *Biomolecules* **2019**, *9*, 330.
(73) Chis, A. A.; Dobrea, C.; Morgovan, C.; Arseniu, A. M.; Rus, L. L.; Butuca, A.; Juncan, A. M.; Totan, M.; Vonica-Tincu, A. L.; Cormos, G.; Muntean, A. C.; Muresan, M. L.; Gligor, F. G.; Frum, A. Applications and Limitations of Dendrimers in Biomedicine. *Molecules* **2020**, *25*, 3982.
(74) Sebestik, J.; Niederhafner, P.; Jezek, J. Peptide and glycopeptide dendrimers and analogous dendrimeric structures and their biomedical applications. *Amino Acids* **2011**, *40*, 301−370.
(75) Wrobel, D.; Appelhans, D.; Signorelli, M.; Wiesner, B.; Fessas, D.; Scheler, U.; Voit, B.; Maly, J. Interaction study between maltose-modified PPI dendrimers and lipidic model membranes. *Biochim. Biophys. Acta, Biomembr.* **2015**, *1848*, 1490−1501.
(76) Zhang, C.; Pan, D.; Luo, K.; Li, N.; Guo, C.; Zheng, X.; Gu, Z. Dendrimer−doxorubicin conjugate as enzyme-sensitive and polymeric nanoscale drug delivery vehicle for ovarian cancer therapy. *Polym. Chem.* **2014**, *5*, 5227−5235.
(77) Andrew MacKay, J.; Chen, M.; McDaniel, J. R.; Liu, W.; Simnick, A. J.; Chilkoti, A. Self-assembling chimeric polypeptide−doxorubicin conjugate nanoparticles that abolish tumours after a single injection. *Nat. Mater.* **2009**, *8*, 993−999.
(78) Lakowicz, J. R. *Principles of fluorescence spectroscopy*; Springer, 2006.
(79) Karukstis, K. K.; Thompson, E. H.; Whiles, J. A.; Rosenfeld, R. J. Deciphering the fluorescence signature of daunomycin and doxorubicin. *Biophys. Chem.* **1998**, *73*, 249−263.
(80) Maji, D.; Lu, J.; Sarder, P.; Schmieder, A. H.; Cui, G.; Yang, X.; Pan, D.; Lew, M. D.; Achilefu, S.; Lanza, G. M. Cellular Trafficking of Sn-2 Phosphatidylcholine Prodrugs Studied with Fluorescence Lifetime Imaging and Super-resolution Microscopy. *Precis. Nanomed.* **2018**, *1*, 128−145.
(81) Gonçalves, M.; Mignani, S.; Rodrigues, J.; Tomás, H. A glance over doxorubicin based-nanotherapeutics: From proof-of-concept studies to solutions in the market. *J. Controlled Release* **2020**, *317*, 347−374.
(82) Zhang, X.; Lin, Y.; Gillies, R. J. Tumor pH and Its Measurement. *J. Nucl. Med.* **2010**, *51*, 1167−1170.
(83) Alves, C.; Magarkar, A.; Horta, M.; Lima, J.; Bunker, A.; Nunes, C.; Reis, S. Influence of doxorubicin on model cell membrane properties: Insights from in vitro and in silico studies. *Sci. Rep.* **2017**, *7*, 6343.
(84) Wang, J.; Li, D.; Fan, Y.; Shi, M.; Yang, Y.; Wang, L.; Peng, Y.; Shen, M.; Shi, X. Core−shell tecto dendrimers formed via host−guest supramolecular assembly as pH-responsive intelligent carriers for enhanced anticancer drug delivery. *Nanoscale* **2019**, *11*, 22343−22350.
(85) Wang, G.; Fu, L.; Walker, A.; Chen, X.; Lovejoy, D. B.; Hao, M.; Lee, A.; Chung, R.; Rizos, H.; Irvine, M.; Zheng, M.; Liu, X.; Lu, Y.; Shi, B. Label-Free Fluorescent Poly(amidoamine) Dendrimer for Traceable and Controlled Drug Delivery. *Biomacromolecules* **2019**, *20*, 2148−2158.
(86) Cummings, J.; Bartoszek, A.; Smyth, J. F. Determination of covalent binding to intact DNA, RNA, and oligonucleotides by intercalating anticancer drugs using high-performance liquid chromatography. Studies with doxorubicin and NADPH cytochrome P-450 reductase. *Anal. Biochem.* **1991**, *194*, 146−155.
(87) Farhane, Z.; Bonnier, F.; Byrne, H. J. Monitoring doxorubicin cellular uptake and trafficking using in vitro Raman microspectroscopy: short and long time exposure effects on lung cancer cell lines. *Anal. Bioanal. Chem.* **2017**, *409*, 1333−1346.
(88) Yang, F.; Teves, S. S.; Kemp, C. J.; Henikoff, S. Doxorubicin, DNA torsion, and chromatin dynamics. *Biochim. Biophys. Acta* **2014**, *1845*, 84−89.
(89) Kim, H.-J.; Jeung, D.-G.; Oh, J.-M. Boosting the anticancer activity of doxorubicin with a layered double hydroxide nanocarrier. *Appl. Clay Sci.* **2021**, *203*, No. 106000.
(90) Lai, P. S.; Lou, P. J.; Peng, C. L.; Pai, C. L.; Yen, W. N.; Huang, M. Y.; Young, T. H.; Shieh, M. J. Doxorubicin delivery by polyamidoamine dendrimer conjugation and photochemical internalization for cancer therapy. *J. Controlled Release* **2007**, *122*, 39−46.
(91) Zhang, M.; Zhu, J.; Zheng, Y.; Guo, R.; Wang, S.; Mignani, S.; Caminade, A. M.; Majoral, J. P.; Shi, X. Doxorubicin-Conjugated PAMAM Dendrimers for pH-Responsive Drug Release and Folic Acid-Targeted Cancer Therapy. *Pharmaceutics* **2018**, *10*, 162.

https://doi.org/10.1021/acs.biomac.1c01264
Biomacromolecules 2022, 23, 276−290